ANALYSIS AND SIMULATION IN NEURON AND FIBROSIS MODELS

by

HUMBERTO D. PEREZ GONZALEZ

Presented to the Faculty of the Graduate School of

The University of Texas at Arlington in Partial Fulfillment

of the Requirements

for the Degree of

DOCTOR OF PHILOSOPHY

THE UNIVERSITY OF TEXAS AT ARLINGTON

August 2009

To Humberto and María, my parents. Thanks for all you have done for me.

***

A Humberto y María, mis padres. Gracias por todo lo que han hecho por mi.

ACKNOWLEDGEMENTS

I would like to thank my supervising professor Dr. Jianzhong Su for constantly motivating and encouraging me, and also for his invaluable advice during the course of my doctoral studies. I wish to thank Dr. Tuncay Aktosun, Dr. Yue Liu, Dr. Gaik Ambartsoumian, and Dr. Benito Chen for their interest in my research and for taking time to serve in my dissertation committee.

July 27th, 2009

ABSTRACT

ANALYSIS AND SIMULATION IN NEURON AND FIBROSIS MODELS

Humberto D. Perez Gonzalez, Ph.D.

The University of Texas at Arlington, 2009

Supervising Professor: Jianzhong Su

In this work, we use analysis and numerical simulations to study the change of collective behavior of two synaptically coupled square bursting systems, the effect of noise in an elliptic bursting system and foreign body reactions. For the square bursters we study its synchronization process as the strength of coupling increases. The two cells present chaotic bursting behavior when there is no coupling. As the strength increases and past a certain value, the behavior of two cells, which are uncoupled, becomes synchronized regular bursting motions. For the elliptic bursting phenomenon we study the distribution of the noise and its effects in the dynamics and the reliability of the firing pattern. Finally, we study foreign body reactions to implants. A computational model is constructed to investigate the time dynamics of the reaction kinetics of the major elements involved in the fibrosis formation process.

TABLE OF CONTENTS

LIST OF FIGURES

LIST OF TABLES

CHAPTER 1

INTRODUCTION

In this work we study the change of collective behavior of two synaptically coupled square bursting systems, the effect of noise in an elliptic bursting system and modeling and simulation of foreign body reactions due to implants.

First, we study the change of collective behavior of two synaptically coupled square bursting systems as the strength of coupling increases. The two cells present chaotic bursting behavior when there is no coupling. We showed analytically that the quotient of the time difference in the slow manifold after one loop is a contraction, which implies that the behavior of the two cells becomes synchronized regular bursting motions. It also shows that regular oscillations can emerge from connecting intrinsically chaotic oscillators with synapses. The method of analysis is similar to that of Fast Threshold Modulation theory in [82].

Next, we study the behavior of elliptic burster in the presence of noise. We start with an introduction to a geometric analysis of elliptic bursting with and without noise. The basic technique is to establish an invariant region for the return map of the solutions. For noisy elliptic bursters, the bursting patterns depend on random variations associated with delayed bifurcations. Details for the most important results are provided from [92]. In that paper an explicit formulation of the duration of delay and its distribution is provided. The duration of the delay, and consequently the durations of active and silent phases, is shown to be closely related to the logarithm of the amplitude of the noise. As a continuation of this part, we studied the reliability of the firing pattern.

Finally, we study the foreign body reactions to implants. Foreign body reactions are commonly referred to the network of immune and inflammatory reactions of human or animals to foreign objects placed within tissues. They have significant relevance to bioengineering implant material design and fabrication, as fibrotic capsulations to implants within human or animals are found to substantially reduce the effectiveness of the devices. This study focuses on a kinetic based predictive tool in order to analyze the outcome of multiple interactive cell-protein complex kinetics of various factors and processes and to understand its transient behavior during the entire period (up to several months). A computational model is constructed to investigate the time dynamics of the reaction kinetics. The simulation results have been consistent with experimental data and the model can facilitate quantitative information for study of foreign body reaction process.

CHAPTER 2

REGULAR BURSTING IN COUPLED CHAOTIC NEURONS

2.1 Background

Burst activity is characterize by slowly alternating phases of near steady state behavior and trains of rapid spike oscillations (See Figure 2.1). These two phases have been called the silent and active phases respectively. In the case of electrical activity of biological membrane systems the slow time scale of bursting is in the order of tens of second while the spikes have milliseconds time scales [68]. Rinzel and Wang [105] describe qualitatively some mechanisms for burst generation. The basic idea is that there are slow processes which modulate the faster spike generating dynamics. To classify burst patterns they consider systems of the form

$$\begin{aligned} \mathbf{x}' &= F(\mathbf{x}, \mathbf{y}), \quad \mathbf{x} \in \mathbb{R}^n, \qquad \text{(FAST)} \\ \mathbf{y}' &= \varepsilon G(\mathbf{x}, \mathbf{y}), \quad \mathbf{x} \in \mathbb{R}^m \qquad \text{(SLOW)} \end{aligned}$$

with $0 < \varepsilon << 1$.

A global bifurcation analysis of the fast subsystem, taking the slow variables as parameters, gives the structures that matches the different observed patterns that arise from biological membrane systems. In this case ε represents the ratio of fast/slow system time scales. There are some common denominations for these burst patterns. A more detailed description is given in [105]. Here we only mention the main characteristics of square and elliptic bursting.

- **Square bursting:** It presents a square-like wave (Figure 2.1B, right). It is based on a bistability of a steady state and a repetitive firing state in the fast subsystem and periodic switching between the two (Figure 2.1B, middle).
- **Elliptic bursting:** It involves a subcritical Hopf bifurcation in the fast subsystem. Bursting involves slow switching between a steady state and a repetitive firing state that are bistable in the fast subsystem (Figure 2.1D, middle). The silent phase exhibits damped or growing oscillations (elliptic) as its trajectory passes through the Hopf bifurcation point (Figure 2.1D, right).

So, neurons are modeled by fast-slow dynamical systems and we simulated its behavior in a network by a system of coupled differential equations. By analyzing this system we expect to gain some insight about the dynamics of neurons when they are interacting in its natural environment. Event thought the analysis of these dynamical systems can be described in a generic way, we have borrowed some terminology from neurophysiology to describe it.

Remark 1.

The bifurcation diagrams of the fast subsystem in this chapter and chapter 3 were computed using the program XPPAUT by Ermentrout [21]. It uses AUTO, written by Doedel, to do continuation of parameters.

We consider a system of two synaptically coupled Hodgkin-Huxley type neurons and we intend to study its dynamical behavior. The system models the collective behavior of two neuron cells coupled through synapses whose actions potentials are due to release of neural transmitters. Quantitatively, the synapse is approximated by a Heaviside function. An individual cell here presents a chaotic dynamics and has solutions with distinct patterns that appear in two time scales, called bursting. In this part, each of the systems is assumed to be identical to other, and individually it presents the typical square bursting as described by Rinzel [68], Terman [98] and

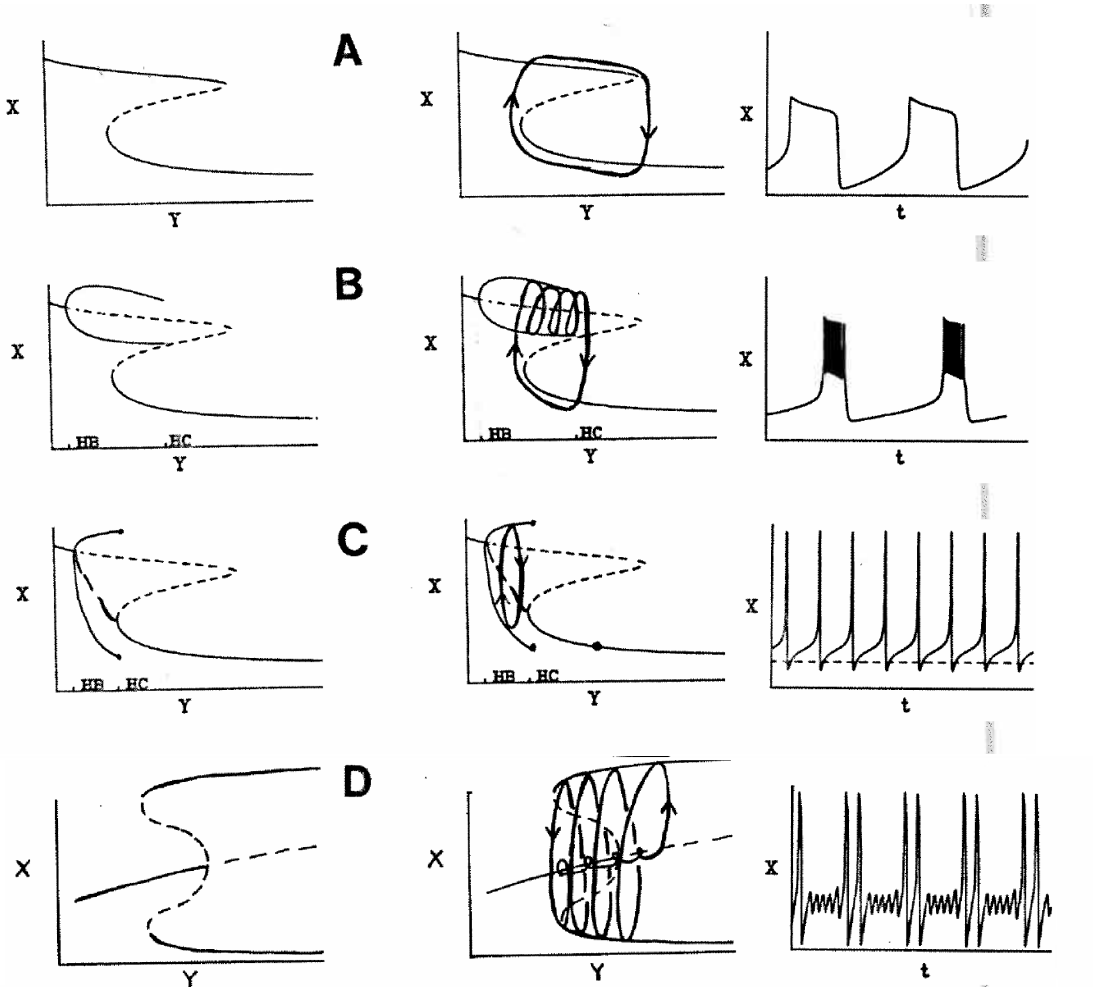

Figure 2.1: Left: Bifurcation diagram of periodic and steady state solutions to fast subsystem (FAST) with slow variables as parameters. Maximum and minimum of periodic solutions are plotted. Unstable solution indicated by short dashes. Center: Schematic representation (thick curves) of slow waves, bursts or continuous spiking trajectory as projected on bifurcation diagram of the corresponding left panel. Right: Time course of a fast variable for the corresponding center panel. Homoclinic bifurcations (HC) and Hopf bifurcations (HB) are also indicated. This figure was adapted from Fig. 1 and Fig. 2 in [68].

Sherman and Rinzel [78]. It was known [98] that at certain parameter range, some chaotic characters of solutions occur. However when two identical chaotic systems are coupled together, there are many possibilities. They could either synchronize into an in-phase solution or an out-of phase solution, or neither, depending on the parameter range and the method of coupling. For example, Sherman and Rinzel [78] showed two neurons with diffusive coupling (gap junction in neuroscience terms) may have a much longer active phase of high frequency oscillations than a single neuron of the same property. There were intensive studies of diffusively coupled regular or chaotic neurons available in the literature but they are out of the scope of our study. The mathematical study of synaptically coupled cells started from the Fast Threshold Modulation Theory, initiated by Somers and Kopell [82]. Rubin and Terman [73] had also described in detail how to analyze the synchronization of neurons by a geometric method for differential equation. Some recent studies can be found in [17] and [20].

We study a synaptically coupled system of two identical Hodgkin-Huxley type neurons . When there is no coupling or weak coupling, the systems appear with a focus in chaotic behavior and unsynchronized. But when the synaptic coupling strength is large enough, the systems will be regular and synchronized. The phenomenon was observed by Abarbanel et al and was confirmed by calculating Lyaponov exponents in [1]. Through analyzing its fast and slow manifolds, we provide the underlining mechanism of this phenomenon from a different perspective. Regularizing chaotic cells can also be possible by an averaged coupling in [74] which is not related to our study.

We organized this section in the following way: In Section 2.2, we start with general assumptions and discuss the individual behavior of a single system. In Sections 2.3 and 2.4, we consider the dynamical behavior of the systems with a coupling that leads to synchronization and regularization. A brief discussion is in Section 2.5.

2.2 General Assumptions on Individual Neuron

For simplicity, we assume that individual neurons are identical in our case. In our model, motivated by Hodgkin-Huxley equation (or its variation such as FitzHugh-Nagumo model, Hindmarsh-Rose model) [68], the intracellular membrane potential and currents of neuron satisfy the differential equations:

$$v' = f_1(v, w, y) \tag{2.1a}$$

$$w' = f_2(v, w, y) \tag{2.1b}$$

$$y' = \varepsilon g(v, w, y). \tag{2.1c}$$

The sub-system containing the first two equations (2.1a-2.1b) is called the fast sub-system (FS). The last equation (2.1c) is called the slow equation. We assume

(H1) The set of steady states of (FS) consist of an S-shaped curve of y in (v, y)-plane denoted by S. There exists y_λ and y_ρ such that the number of steady states of (FS) equals to 1 as $y \in (-\infty, y_\lambda)$, equals to 3 as $y \in (y_\lambda, y_\rho)$, equals to 1 as $y \in (y_\rho, \infty)$. Denote the right knee (located on the lower branch) by $P_\rho = (v_\rho, w_\rho, y_\rho)$ and left knee on upper branch $P_\lambda = (v_\lambda, w_\lambda, y_\lambda)$. We also denote the upper, middle and lower branch of S by U, M, L.

(H2) We further assume that the lower branch L consist of stable steady states for (FS) and the middle branch consist of steady states which are saddles for (FS). The upper branch is more complicated than the cases considered in Terman [98]. For two intervals $y_b \leq y < y_h$ and $y_H < y \leq y_B$, there exists one-parameter families of periodic solutions of FS, denoted by P_1 and P_2 respectively. Both P_1 and P_2 have a Hopf bifurcation point at one end, and they both terminate at a homoclinic orbit from saddle points at the middle branch. These homoclinic

points are denoted as $p_h = (v_h, w_h, y_h)$ and $p_H = (v_H, w_H, y_H)$. See Figure 2.2. Both P_1 and P_2 are stable for (FS) with y-fixed.

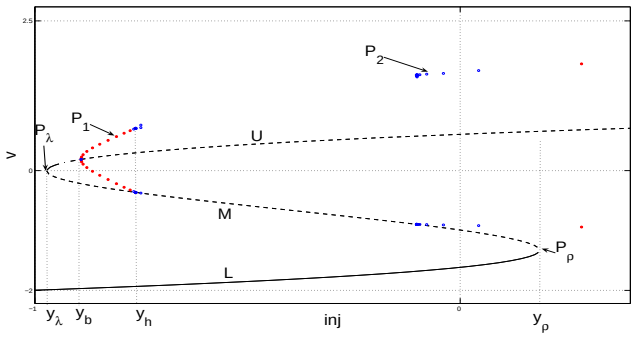

Figure 2.2: Bifurcation diagram of the Fast Subsystem (FS) for Equation 2.2

(H3) For slow dynamics, the y-dependent nullsurface $N \equiv \{(v, w, y)|g = 0\}$ intersect the curve S at a unique point below p_h and further down M towards P_ρ, and N is quite close to P_ρ in distance. As typical, $U \subset \{g < 0\}$, $P_1(t) \subset \{g < 0\}$ and $P_2(t) \subset \{g < 0\}$ while $L \subset \{g > 0\}$. We assure the point P_ρ is nondegenerate described as follows [49]. Let $F = (f_1, f_2)$. Then $DF_x(P_\rho)$ has one negative eigenvalue and one zero eigenvalue. Further, Let η, χ be the eigenvectors corresponding to the zero eigenvalue of $D_xF(P_\rho)$ and $(D_xF(P_\rho))^T$, we have $< \chi, D_xF(P_\rho) > \neq 0$ and $< \chi, D_{xx}F(P_\rho)(\eta, \eta) > \neq 0$. Assumptions on P_λ are similar. Geometrically, it implies that P_ρ and P_λ behave like parabolas. We also assume that there exists a unique stable trajectory r_ρ such that $r_\rho(t) \to P_\rho$ as $t \to -\infty$ and $r_\rho(t) \to P_2(t)$ as $t \to \infty$ for (FS). Similar assumption holds for P_λ.

With the assumptions given above, the behavior of a single cell is well understood by Terman [98] and Lee and Terman [49]. We introduce two basic results.

Theorem 1 (Terman [98] and Lee and Terman [49]). *Assume H1-H3 hold for Equation 1. There exists $\varepsilon_i \to 0^+$ as $n \to \infty$ and $\delta_i \leq C_i e^{-k/\varepsilon_i}$, the periodic bursting solution that alternates between L and P_2, is uniquely determined and asymptotically stable for all $\varepsilon > 0$ except for $\varepsilon \in \cup_i(\varepsilon_i - \delta_i, \varepsilon_i + \delta_i)$.*

The bursting solutions mentioned above are regular solutions without chaotic motions. In cases of our interest, the solutions behave chaotically. In previous study of Terman [98], the null function $g(v, w, y)$ is linearly dependent on a parameter k, that is glucose level in pancreatic model. The parameter k can be adjusted such that when k is small, Equation 2.1 gives rise to regular bursting solutions and when k is above a certain value, Equation 2.1 has continuous spikes. In the (ε, k)-plane, there is a wedge region where the corresponding Poincaré Mapping induced by Equation 2.1 presents a Fibonacci dynamics that characterizes the chaotic dynamics.

Theorem 2 (Terman [98]). *Assume H1-H3 hold for Equation 1. The chaotic bursting solutions exist for all $\varepsilon > 0$ and for $k = k(\varepsilon)$. There exists an integer $N = N(\varepsilon)$ and real numbers $\{k_j\}, 1 \leq j \leq N(\varepsilon)$ with $k_j \leq k_{j+1}$ such that for $k \in [k_{2j}, k_{2j+1}]$ the return mapping $\pi(k, \varepsilon)$ near the lower branch of the steady state of the fast subsystem at $y = y_H$ gives rise to a j-Fibonacci dynamics.*

Several neuron cells have those characters we mentioned above. For example, Morris-Lecar model [98] and Hindmarsh-Ross model (HR) [1] all satisfy the assumptions mentioned earlier. In this study, we will investigate HR (a prototype for Hodgkin-Huxley theory) numerically using XPPAUT software to motivate our study of coupled systems. The biological meaning of the assumptions were carefully explained in [98] and [78]. The variable v represents the intracellular membrane po-

tential, the variable w is recovery variable and y is inward current. The parameter Inj is the injected current into the neuron:

$$\begin{aligned} v' &= w + \phi(v) - y + Inj \\ w' &= \psi(v) - w, \\ y' &= -\varepsilon(y + S(v - c)) \end{aligned} \tag{2.2}$$

where $Inj = 3.281$, $\varepsilon = 0.0021$, $c = -1.6, S = 4.0$, $\phi(s) = 3s^2 - s^3$, $\psi(s) = 1 - 5s^2$. The initial values are set at $v = 0$, $w = 0$, $y = -2$. Figure 2.3 shows a chaotic bursting trajectory of Equation 2.2.

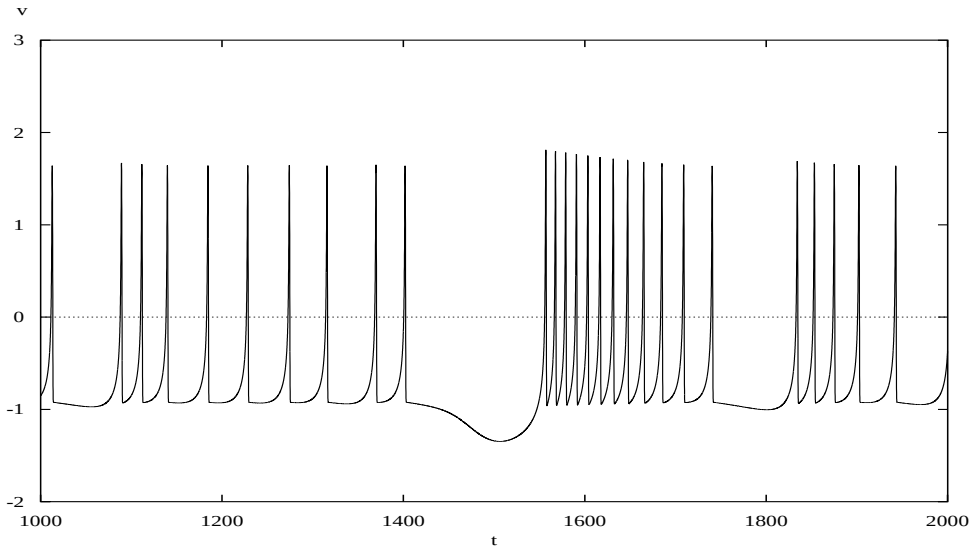

Figure 2.3: A chaotic trajectory of Equation 2.2

2.3 Coupled Oscillators

There are a number of ways by which neurons can communicate to each other. Two most common mechanism are diffusive coupling (gap junction) or synaptic coupling through neural transmitters. Roughly speaking, a diffusive coupling models a

direct electric connection through two neurons, and synaptic coupling describes the connection through release of neural transmitters at synapse terminals when other neurons activate.

Motivated by the work of Somers and Kopell [82] and Abarbanel et al[1], we consider the coupled systems:

$$\begin{aligned} v_1' &= f_1(v_1, w_1, y_1) + \alpha(-v_1 - V_c)H(X_c + v_2) \\ w_1' &= f_2(v_1, w_1, y_1) \\ y_1' &= \varepsilon g(v_1, w_1, y_1) \\ v_2' &= f_1(v_2, w_2, y_2) + \alpha(-v_2 - V_c)H(X_c + v_1) \\ w_2' &= f_2(v_2, w_2, y_2) \\ y_2' &= \varepsilon g(v_2, w_2, y_2). \end{aligned} \tag{2.3}$$

We denote $U_1 = (v_1, w_1, y_1)$, and $U_2 = (v_2, w_2, y_2)$. The constant parameter $\alpha > 0$ represents the strength of the coupling. Reminding that L is the lower branch of the single cell. For $U_1 \in L, U_2 \in L$, we have $(-v_1 - V_c) > 0, (-v_2 - V_c) > 0$ and therefore the couplings are excitatory [82]. The function $H(\cdot)$ is the Heaviside Function and $(-X_c)$ is the threshold. Although the discontinuous Heaviside Function is used, systems with smoothed version of H yield to similar results.

We study first the numerical solutions of the coupled HR model

$$\begin{aligned} v' &= w + \phi(v) - y + Inj - \alpha(v + 1.4)H(V + 0.85) \\ w' &= \psi(v) - w \\ y' &= -\varepsilon(y + S(v - c)) \\ V' &= W + \phi(V) - Y + Inj - \alpha(V + 1.4)H(v + 0.85) \\ W' &= \psi(V) - W \\ Y' &= -\varepsilon(Y + S(V - c)) \end{aligned} \tag{2.4}$$

where all conditions in Equation 2.2 hold and initial conditions $V = 0, W = 0.2, Y = -3.02$. The coupling strength α is set at 0.2. We find that the solutions will quickly synchronize into a bursting solution that is regular and attracting, as shown in Figure 2.4. The simulations for Equation 2.4 suggested that the behavior of solutions, with a strong coupling $\alpha > \alpha_0$, will result in regular periodical bursting, and solutions of different initial positions will synchronize as t goes to infinity.

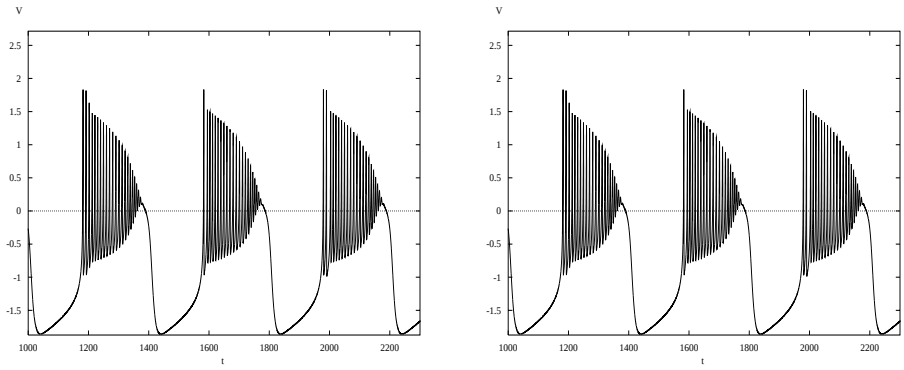

Figure 2.4: Convergence to a periodic regular bursting solution

We denote the family of solutions $S_\alpha(y)$ to be the steady states of (FS) for the synchronized system Equation 2.5

$$\begin{aligned} v' &= f_1(v, w, y) - \alpha(v + V_c) \\ w' &= f_2(v, w, y) \\ y' &= \varepsilon g(v, w, y). \end{aligned} \tag{2.5}$$

The numerical calculation of the bifurcation for (FS) of Equation 2.5 indicated that when $\alpha > \alpha_0^-$, the family of periodic solutions P_1 and P_2 will be detached from the middle branch and will merge into one continuous branch P_α. The periodic family P_α will start from one Hopf bifurcation and terminate at another Hopf-bifurcation at its upper branch at $y = y_b$ and at $y = y_B$, as shown in Graph 2.5.

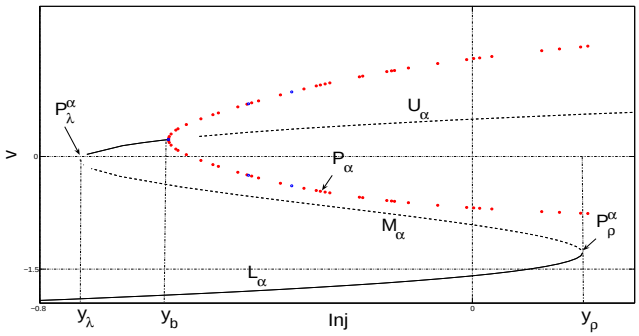

Figure 2.5: The bifurcation diagram of (FS) for Equation 2.5 for the particular example of (HR, Equation 2.2, $\alpha = 0.2$, $V_c = 1.4$

We denote the upper branch of the new bifurcation diagram U_α and the lower branch L_α. We now state our final two assumptions.

(H4) Suppose that there exists a unique value α_0 such that as $\alpha \to \alpha_0^-$, both y_h and y_H collapse to each other. If $\alpha > \alpha_0$, then the family of periodic solution P_α will be separated from the middle branch.

(H5) The coupling strength α is chosen so that the left knee P_λ^α is between the gap of P_1 and P_2 i.e., $y_h < y_\lambda^\alpha < y_H$. This restricts the value α of coupling strength.

2.4 Synchronization to Regular Bursting Solutions

We denote F to be the union of all fast manifolds from L to U or P_2, and from U or P_2 to L for Equation 2.4. Similarly, let F_α be the union of all fast manifolds from L_α to U_α or P_α, and from U_α or P_α to L_α for Equation 2.6.

Theorem 3 (Main Result. Su, Perez and He)**.** *Suppose H1-H5 hold. There exists a periodic solution $U(t,\varepsilon,\alpha)$ with period $T(\varepsilon,\alpha)$ for Equation 2.3 such that*

(1) dist$(U(t,\varepsilon,\alpha), L\cup F\cup P_\alpha\cup U_\alpha\cup F_\alpha) = O(\varepsilon)$, and $\lim_{\varepsilon\to 0} T(\varepsilon,\alpha) = T_0(\alpha) > 0$.

(2) there exits $\delta > 0, t_0 > 0$ such that when any pair of coupled bursting solutions (v_i, w_i, y_i), $i = 1, 2$ with initial conditions satisfying

$$|(v_1,w_1,y_1)(0) - (v_2,w_2,y_2)(0)| \le \delta, \quad |(v_i,w_i,y_i)(t) - U(t+t_0,\varepsilon,\alpha)| \le M_0 e^{-c_0 t}$$

for $t > t_0, i = 1, 2$, i.e. both bursting solutions synchronize to the periodic solution $U(t,\varepsilon,\alpha)$ with a time shift t_0.

An Outline of Proof for Theorem 3. Analyzing the solutions, we note that the slow manifold L is stable with respect to (FS). Namely, The linearized operator of (FS) near L has two negative real eigenvalues except near the right knee for Equation 2.1. For $y_b^\alpha \le y \le y_B^\alpha$, the branch $U_\alpha(y)$ is circled by $P_\alpha(y)$ from outside. Along both sections of $U_\alpha(y)$ to the left and to the right of $P_\alpha(y)$, the operator from (FS) of Equation 2.5 has a pair of complex eigenvalues of negative real parts, except for the left knee P_λ^α. For the periodic branch P_α, the Floquet multiplier are 1 and $\mu, |\mu| < 1$. We use the classical results from Fenichel [27] to assert the existence of invariant manifolds near the slow manifold and only analyze the flows within the neighborhood

of the invariant manifolds L, U_α and P_α. Note that the solutions follow L rather than L_α because $H \equiv 0$ when both cells are in lower branch.

We start both solutions of Equation 2.3 at different initial points at the lower branch L. Without loss of generality, let $U_1(t)|_{t=0}$ be at the right knee P_ρ and $(y_1(t) - y_2(t))|_{t=0} = z > O(\sqrt{\varepsilon})$, $z = O(\alpha)$ is independent of ε. Further $y_2(t)|_{t=0}$ is to the right of P_ρ^α, the right knee of the bifurcation diagram in Equation 2.5 with $\alpha > 0$. Because this is a restrictive condition on the initial position difference, our result is a local synchronization.

Since the nature of the coupling there is excitatory, in the terminology of Somers et al [82], both trajectories will move up to the periodic family P_α through the following sequence of events.

(a) For $0 \equiv t_1 \leq t \leq t_2(\varepsilon) = t_1 + O(\frac{1}{\sqrt{\varepsilon}})$, $U_1(t) \in N(F)$ i.e., within the ε-neighborhood of L and $v_1 \leq (-X_c)$ while $U_2(t) \in N(L)$, i.e. the solution U_1 leaves the right knee and moves up along the fast manifold F (discussed earlier, and also see [57]) but it is still below the threshold $(-X_c)$ to influence the second neuron; the second solution U_2 remains the lower branch for the time being.

(b) For $t_2 \leq t \leq t_3(\varepsilon) = t_2 + O(\frac{1}{\sqrt{\varepsilon}})$, $U_1(t) \in N(F \cup P_2)$ and $v_1(t) > -X_c$, while $U_2(t) \in N(F)$ but $v_2(t) < -X_c$ below the threshold i.e., the solution U_1 goes past the threshold and eventually reaches P_2 the family of periodic solutions on the upper branch of unexcited equation. The second solution U_2 leaves from the lower branch to move up to the fast manifold F, because U_2 gets excited after U_1 goes above the threshold.

(c) For $t_3 \leq t \leq t_4(\varepsilon) \leq t_3 + O(1)$, while $U_2(t) \in N(F)$ and $v_2(t) > -X_c$ is above the threshold, $U_1(t)$ jumps away from $N(P_2)$ and goes to $N(P_\alpha)$, the new periodic family of the synchronized system.

(d) For $t_4 \leq t \leq t_5(\varepsilon) \leq t_4 + O(1)$, $U_1(t)$ stays within $N(P_\alpha)$, while $U_2(t) \in N(F_\alpha)$ and $U_2(t_5) \in N(P_\alpha)$ i.e., the solution U_2 jumps to the family of periodic solutions on the upper branch of excited equation.

(e) Finally as $t > t_5$, both $U_1(t)$ and $U_2(t)$ settle on P_α, then $|y_1(t_5) - y_2(t_5)| = z + O(\sqrt{\varepsilon})$. Note $U_1(t)$ and $U_2(t)$ can switch positions during the jump [82].

We remark that when the solutions move along the slow manifolds L, P_α, U_α, the time difference between the solutions is invariant, because the systems are decoupled and the two neurons are identical systems. However the time difference between U_1 and U_2 has certainly changed substantially during the jump up and jump down between slow manifolds via a fast manifold F, even though the phase difference in y-value remain invariant (up to a precision of $O(\sqrt{\varepsilon})$). We now calculate the time difference by tracking the dynamics on slow manifolds (the lower branch, the upper branch as well as the periodic family).

For the lower branch, the slow dynamics satisfies the equation:

$$\begin{aligned} (v, w)(y) &= L(y), \\ y' &= \varepsilon g(L(y), y), \end{aligned} \tag{2.6}$$

the time difference in the lower branch is $\Delta T = \int_{y_\rho - z}^{y_\rho} \frac{1}{\varepsilon g(L(y), y)}\, dy$ where y_ρ is the parameter value for the right knee. Then on the slow manifold along the periodic family P_α, around the upper branch of the excited equations, we use the averaging method [76] to get the slow dynamics for y:

$$\begin{aligned} (v, w)(y) &= P_\alpha(t, y) \\ y' &= \varepsilon g(\bar{P}_\alpha(y), y) + O(\varepsilon^2), \end{aligned} \tag{2.7}$$

where the average motion $\bar{P}_\alpha(y) = \frac{1}{\pi(y)} \int_0^{\pi(y)} P_\alpha(t, y)\, dt$ is the averaged over the period $\pi(y)$. Then the time difference on the periodic branch can also be similarly determined as $\Delta T' = \int_{y_\rho}^{y_\rho - z} \frac{1}{\varepsilon g(\bar{P}_\alpha(y), y)}\, dy$.

We now consider that both U_1 and U_2 move along P_α while maintaining time difference invariant and eventually enter U_α, the upper branch to the left of Hopf bifurcation point. They will come near the left knee point P_λ^α. Either U_1 or U_2 will lead the way as they go through the left knee and eventually jump down to the lower branch L in a similar scenario as in the jumping-ups of U_1 and U_2. The reason of jumping downs, however, is different. The couplings there are not excitatory. When one falls below $-X_c$, the other one is near the left knee of U_α and now follows F_α and then F. Because of H3 and H5, both U_1 and U_2 will move down to the only stable steady state L.

Similarly, we can calculate from the invariant time difference $\Delta T'' = \Delta T'$ when traveling along the upper branch U_α to obtain a horizontal phase difference $\tilde{z}$ at the left knee. Also, $\Delta T'''$, the time difference traveling along the lower branch L can be calculated from the horizontal phase difference $\tilde{z}$, because the phase difference is invariant during jumping down.

Now, we summarize by calculating the change of time difference between two neurons for one loop. We note that during the jump, the y-difference is invariant (up to an error of $O(\sqrt{\varepsilon})$), and when traveling in upper or lower branches, the t-difference is invariant. Let the initial difference z be sufficiently small, we have $\Delta T = (\frac{1}{\varepsilon g(L(y), y)}|_{y=y_\rho})z + \text{h.o.t}$, $\Delta T' = (\frac{-1}{\varepsilon g(P_\alpha(y), y)}|_{y=y_\rho})z + \text{h.o.t}$, Then the time difference of ΔT will translate into the phase difference of $\tilde{z}$ at the left knee $\Delta T' = \Delta T'' = (\frac{-1}{\varepsilon g(U_\alpha(y), y)}|_{y=y_\lambda})\tilde{z} + \text{h.o.t}$ and the final time difference after returning to L is $\Delta T''' = (\frac{1}{\varepsilon g(L(y), y)}|_{y=y_\lambda})\tilde{z} + \text{h.o.t}$. We note here that because of the Heaviside function type

coupling, the systems are decoupled if they are both in L or U_α and P_α, $\Delta T' = \Delta T''$, this is simpler than the direct or indirect synapse cases studied by Terman et al [101].

Therefore we drive the ratio of time difference

$$\frac{\Delta T'''}{\Delta T} = \frac{\Delta T'''}{\Delta T''}\frac{\Delta T''}{\Delta T'}\frac{\Delta T'}{\Delta T} = \frac{g(U_\alpha(y),y)|_{y=y_\lambda} g(L(y),y)|_{y=y_\rho}}{g(L(y),y)|_{y=y_\lambda} g(\bar{P}_\alpha(y),y)|_{y=y_\rho}} + \text{h.o.t.} \equiv \sigma \tag{2.8}$$

When the null surface of g is close to either the right knee of the lower branch L or the left knee of upper branch U_α, the numerator $g(U_\alpha(y),y)|_{y=y_\lambda} g(L(y),y)|_{y=y_\rho}$ is small and $\sigma < 1$. We derive that given any two solutions of initial difference $z \leq z_0$, their time difference will decrease and $\Delta T(t) = O(\sigma^{\frac{t}{\pi_\alpha}})$ where $\pi_\alpha = O(1/\varepsilon)$ is the time duration for traveling on slow manifold L, P_α and U_α once.

Remark: We only discussed simplest scenario in local synchronizations, while there are other possible cases of synchronizations. However it does not necessarily hold global synchronization. It is also possible the two cells are synchronized but the spikes are completely out of phase. On the other hand, the analysis can be carried to a network of N-neurons, the implication there is that all neurons will form several clusters if they are not completely synchronized. The number of cluster will depend on the coupling strength α [102], [73]. □

2.5 Discussion

We are interested in the dynamic patterns that arise during the transition from unsynchronized chaotic actions of neurons to ultimately synchronized regular neuronal activities as we increase the strength of the synaptic coupling. Some numerical experiments suggested the neurons become regular first as we increases the coupling, and then become synchronized. See Figure 2.6 for unsynchronized bursting solution, when $\alpha = 0.05$ in Equation 2.4. It is partially understandable that the parameter

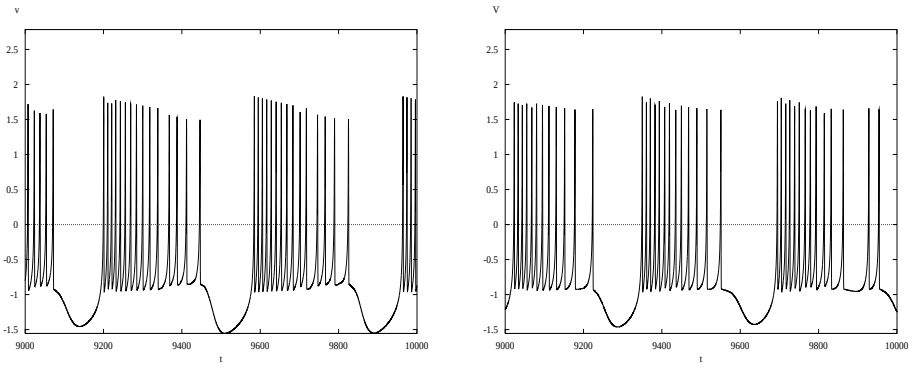

Figure 2.6: For some medium coupling strength, there are regularized bursting solutions of Equation 2.4. The coupling strength is not strong enough to synchronize the solutions.

region for chaotic behavior to occur, U_1 is regular but U_2 is still chaotic, in a single neuron is relatively narrow. However, this behavior involves some transient dynamics that cannot be entirely determined by one neuron alone, the chaotic behavior for coupled systems remains an open question. We plan to further study the transitional range and the evolution of the dynamical behavior of the system of coupled neurons.

These results were published in [94].

CHAPTER 3

EFFECT OF NOISE ON ELLIPTIC BURSTERS

3.1 Background

The main characteristics of the noisy and deterministic elliptic bursters are well described in Su et al. [92] and from there we extracted the most relevant facts about them.

In several brain areas, neurons have been observed experimentally to engage in a rhythmic pattern of behavior referred to as elliptic bursting. In elliptic bursting, neuronal activity alternates between active phases, characterized by large amplitude oscillations, and quiescent phases, associated with oscillations of much smaller amplitudes (see Figure 3.2). Neuronal examples are given in the context of thalamic sleep rhythms and other neuronal systems in [14, 15, 16, 36, 44, 50, 70, 75, 72, 104]. We study a model of elliptic bursting proposed by Rinzel [68] and considered previously both by numerical simulation and by fast-slow dissection in a singular limit [68, 70, 105].

The complications involved in such systems are related to a dynamical phenomenon known as delayed bifurcation or delay of stability loss, defined by Arnold [4]. Solutions stay close to a quasi-steady state as the $O(\varepsilon)$-slow variable passes through a threshold where linear stability is lost. Subsequently, after a substantial $O(1)$ delay, solutions jump away from quasi-steady state. These issues have been studied by many authors [2, 4, 5, 9, 10, 18, 19, 23, 24, 25, 28, 34, 36, 37, 38, 39, 46, 47, 48, 53, 29, 57, 59, 60, 61, 62, 63, 64, 77, 80, 83, 86, 87, 88, 89, 90, 91]. When a system can be reduced to a homogeneous system (i.e., zero is an obvious solution), the delay can be attributed to

a simple contraction of solutions. But in general, more conditions are required for delay. In fact, in the case of slow passage through a simple eigenvalue bifurcation where contraction is also present, the amount of delay can be rather small and may vanish as the slowness goes to zero, as shown in examples by Lebovitz [47, 48], Ahlers [2] and Kapila [39]. The delay in slow passage through a Hopf bifurcation is generically more significant for systems that are analytic in complex time, as shown by Shishkova [80], Neishtadt [59, 64] and many others [5, 19, 28, 80, 83, 86, 87, 88, 89, 90, 91]. Even in this case, however, the amount of delay still relates to many factors, such as nearby singularities and, if external forcing is present, the difference between intrinsic and forcing frequencies [5, 64, 89, 90, 91]. When noise is added, numerical computations [5, 107] and asymptotic methods [43, 44] suggest that the amount of delay is significantly reduced. These results may explain why delay has not been observed in certain noisy environments [38].

When the delayed bifurcation is incorporated into a fast-slow system to model bursting phenomena, repetitive behavior is expected. In fact, for a similar system involving delayed bifurcation, Schecter [77] proved that the Poincaré map contains a fixed point. When noise is introduced, its dynamics changes very drastically, very different from the noisy relaxation oscillators analyzed in [6] where there is no delay in the deterministic system. Some canonical models were proposed by Izhikevich in [37]. A study of Kuske and Baer [44] introduced noise of Brownian motion type into an elliptic bursting system. Depending on the amplitude of the noise, it was found that there are regular patterns of alternations between a long active phase and a long silent phase, regular patterns of alternations between short active and silent phases, as well as irregular patterns of alternations of phases with various time durations (see in particularly Figure 3.2 (e-g) of Kuske and Baer [44]). When the noise amplitude is set to be extremely close to zero, the irregular patterns give way

to a pattern that strongly resembles deterministic elliptic bursting. But even with a noise of quite small magnitude, the irregularity is significant. Kuske and Baer [43, 44] determine that this irregularity follows from random variation in the delay of stability loss, based on an asymptotic approximation of the probability density function for the state of the system in the silent phase and an asymptotic analysis of the effect of noise on transitions out of the active phase. The phenomenon is similar to noisy dynamic pitchfork bifurcation studied earlier by Stocks, Manella and McClintock [83], Swift, Hohenberg and Ahlers [95], Berglund and Gentz [7, 8]. In particular, Berglund and Gentz [7] have given a rigorous analysis for various situations, depending on the amplitude of noise.

For noisy elliptic bursters, bursting patterns depend on random variations associated with delayed bifurcation. The duration of the delay, and consequently the durations of active and silent phases, is shown to be closely related to the logarithm of a distance function that is nearly Gaussian and proportional to the amplitude of the noise.

The phenomenon to be discussed here is different from the chaotic behavior caused by different initial positions of the deterministic dynamics. Rather, the irregular patterns are derived from solutions with the same initial position, as noise properties are varied. Further, solutions with different initial positions behave in similar ways.

In Section 3.2, we state general assumptions on an elliptic bursting model without noise and state the existence result for deterministic bursting solutions. In Sections 3.4 and 3.5, we can find the dynamical behavior of the system with noise and a relationship between the bursting patterns and the amount of delay due to the slow passage through a Hopf bifurcation. The amount of delay will be random but is closely related to a normal distribution.

3.2 General Assumptions and Results on Elliptic Bursters

Our assumptions on the elliptic bursting model are quite general. Following Rinzel [68] and Wang and Rinzel [105], assume the variables v (e.g., the voltage across a membrane), w (e.g., the activation of a fast ionic current through the membrane), and y (e.g., the activation of a slow ionic current) satisfy the differential equations

$$v' = f_1(v, w, y), \tag{3.1a}$$

$$w' = f_2(v, w, y), \tag{3.1b}$$

$$y' = \varepsilon g(v, w, y) \tag{3.1c}$$

where $0 < \varepsilon \ll 1$ and f_1, f_2, g are smooth (see (H4) below). The corresponding system with $\varepsilon = 0$ is called the fast subsystem (FS). Equation 3.1c is called the slow equation (SE).

Assume for the System 3.1 that

(H1) There exists an interval $[y_\lambda, y_\rho]$ of y-values on which the set of equilibria of (FS) is a curve of the form $S = \{U_y \equiv (v_0(y), w_0(y), y) \,|\, y_\lambda \le y \le y_\rho\}$.

(H2) (FS) features a subcritical Hopf bifurcation along S, at $p_H = (v_H, w_H, y_H)$, $y_\lambda < y_H < y_\rho$, with a corresponding saddle-node of periodic orbits for $y = y_r \in (y_H, y_\rho)$. The outer periodic solutions, which we denote as $P_y(t)$ for each y, are stable, while the inner ones are unstable (see Figure 3.1). The family $P \equiv \{P_y(t) \,|\, y_h \le y \le y_r\}$ terminates at $y = y_h < y_H$ (possibly in a homoclinic orbit or in another Hopf bifurcation point). Our analysis will assume that trajectories do not enter the vicinity of y_h. For simplicity, we assume that there are no attractors other than S and P.

(H3) There exists a $y_R > y_r$ such that for $y \in (y_\lambda, y_R)$, the equilibrium curve S belongs in the region $\{g < 0\}$. Along each periodic orbit P_y, the motion of y follows

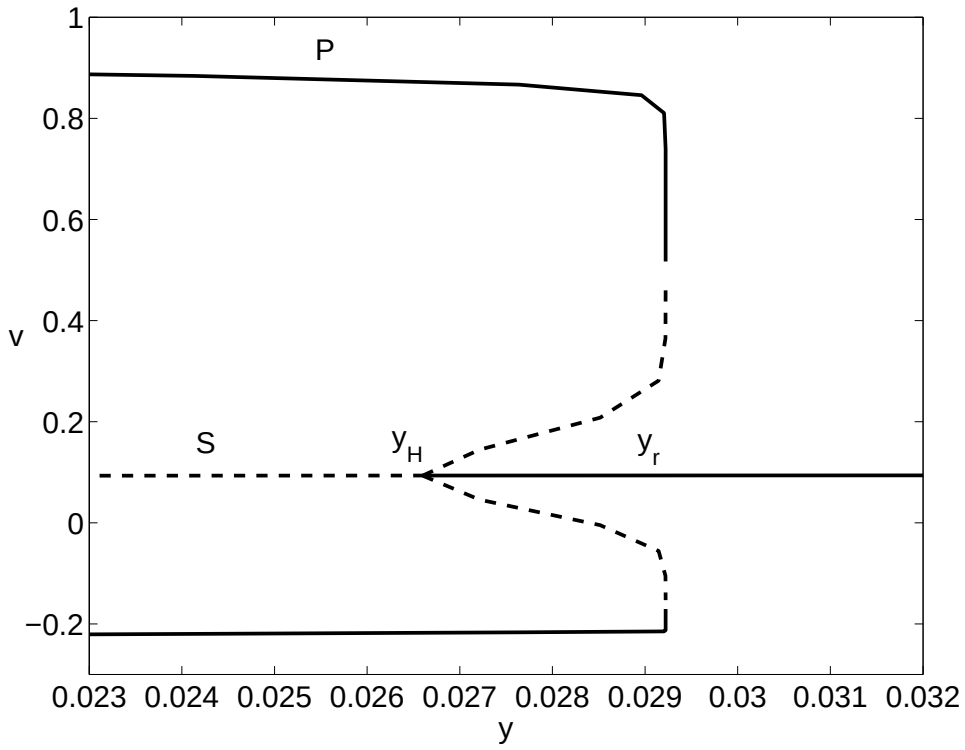

Figure 3.1: Bifurcation diagram for the fast subsystem (FS) of equation (3.1). This particular example was generated numerically from the Wu-Baer model for dendritic spine activity, as discussed in [44] (with parameters given in Figure 3.1 of [44])

an averaged equation derived from (SE). Specifically, we have $y(t) = y_0(t) + O(\varepsilon)$, with y_0 a solution of the averaged equation $y_0{}' = \varepsilon \hat{g}(y_0)$ defined later, and $\hat{g}(y) > 0$ for each $y \in [y_h, y_r]$, we further assume $\hat{g}(y) > 0$ for the inner periodic branch when y is near y_r, which will prevent canard phenomena.

Remark 2.

Define the y-nullsurface $N \equiv \{(v, w, y) \,|\, g = 0\}$. This may intersect S at $y > y_R$, or not at all (as in [44]). In fact, the results below will hold if N intersects S at some y sufficiently far below y_H, as in [70, 72]. We will comment specifically on this case in Remark 4 below.

We make some additional assumptions that are necessary for delayed bifurcation problems. These assumptions are satisfied by the FitzHugh-Nagumo equations and by other neural models under consideration [5, 15, 16, 43, 44, 69, 70, 86, 87].

(H4) The vector functions $f = (f_1, f_2)(v, w, y) : \mathbb{R}^3 \to \mathbb{R}^2$ and $g = g(v, w, y) : \mathbb{R}^3 \to \mathbb{R}$ have analytic extensions in $(v, w, y) \in \mathbb{C}^3$ for $|(v, w)| < \sigma_a$, $|y| < r_a$ in the complex norm for some $\sigma_a, r_a > 0$.

(H5) For each fixed $y \in (y_\lambda, y_\rho)$, the equilibrium curve $(v_0(y), w_0(y))$ is analytic in $y \in \mathbb{C}$ for $|y| < r_a$.

Now, consider the variational equations of (FS) about $(v_0, w_0)(y)$, namely

$$z_t = f_{(v,w)}((v_0, w_0)(y), y)z \tag{3.2}$$

a linear system with coefficients depending on the parameter y.

Let $A(y) = f_{(v,w)}((v_0, w_0)(y), y)$.

(H6) Assume that two eigenvalues of $A(y)$, denoted by $\xi_1(y)$ and $\xi_2(y)$, are complex conjugate to each other i.e., $\xi_2(y) = \bar{\xi}_1(y)$ for each y on the real axis and $|y| < r_a$. Further, near the Hopf bifurcation point y_H, $Re\xi_j(y) < 0$ when $y > y_H$ and $Re\xi_j(y) > 0$ when $y < y_H$. To distinguish the two, we assume that $Im\xi_1(y_H) < 0$. We further assume a transverse crossing occurs, so that $-\frac{dRe\xi_j(y)}{dy} = a_2 > 0$ at y_H.

We define an elliptic bursting solution to be a trajectory that alternates between active phases spent in a certain neighborhood N_P of P, where it undergoes large amplitude oscillations, and silent phases spent in a certain neighborhood N_S of S, where it undergoes small amplitude oscillations. Examples are shown in Figure 3.2.

Under the assumptions (H1)-(H6), we have the existence of elliptic bursting solutions to (3.1).

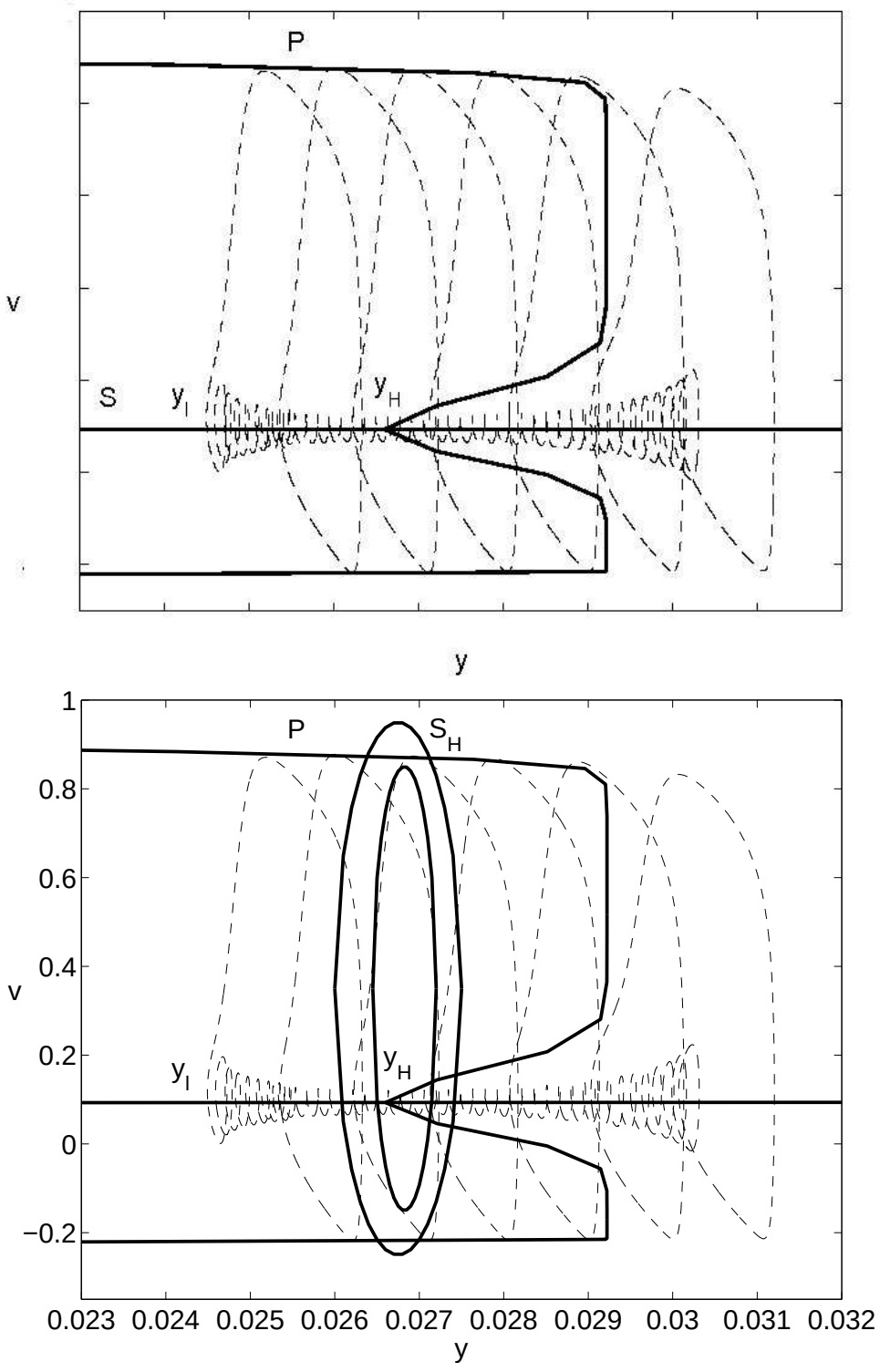

Figure 3.2: (a) (upper). Deterministic elliptic bursting in the Wu-Baer model with parameters from [44] but $\varepsilon = .003$. Note that the y-nullsurface does not intersect S in this model. (b) (bottom). The invariant region S_H.

Theorem 4 (Elliptic bursting)**. a.** *There exists $\varepsilon_0 > 0$ such that the flow induced Poincaré map for equation (3.1) possesses an invariant region S_H, consisting of elliptic bursting solutions, for $0 < \varepsilon \leq \varepsilon_0$. More specifically, S_H is a 2-dimensional ring-shaped invariant region containing P_{y_H}, and further S_H is an absorbing set.*

b. *Each loop time T_ε, that is the time for an elliptic bursting solution to undergo any complete loop from entry into N_S, to entry into N_P, to re-entry into N_S, can be calculated as $T_\varepsilon = T_1 + T_2 + \eta(\varepsilon)$, where T_1, T_2 are $O(\frac{1}{\varepsilon})$ times associated with passage through the silent and active phases, respectively (see equations 3.12) , and* $\lim_{\varepsilon \to 0^+} \varepsilon\eta(\varepsilon) = 0$.

c. *Fix any elliptic bursting solution $(\hat{v}, \hat{w}, \hat{y})$ and time t_1 such that $(\hat{v}, \hat{w}, \hat{y})(t_1) \in S_H$. When $\varepsilon \leq \varepsilon_0$, for any $\delta > 0$ sufficiently small and any solution (v, w, y) of equation (3.1) such that $(v, w, y)(0) \in S_H$ and therefore $y(0) = \hat{y}(t_1) = y_H$, there exists an $M = M(\varepsilon_0) > 0$ such that*

$$|y(t) - \hat{y}(t + t_1)| \leq \delta \tag{3.3}$$

for the time duration $0 \leq t \leq (\frac{\delta}{M\varepsilon|\ln\varepsilon|})(T_1 + T_2 + o(\frac{1}{\varepsilon}))$, corresponding to an $(\frac{\delta}{M\varepsilon|\ln\varepsilon|})$ number of elliptic bursting cycles. Therefore, elliptic bursting solutions are at least metastable.

3.3 Analysis of Deterministic Elliptic Bursters

To understand the dynamics of equation (3.1), we construct neighborhoods N_S for the equilibrium curve S and N_P for the periodic family P. We use (x, y, z) as the

set of new variables in a cylindrical domain diffeomorphic to that of equation (3.1) within N_S. Let $M > 0$ be a constant, and let

$$D = \{(x, u, y) \,|\, x^2 + u^2 \leq (M\varepsilon)^2, |y| \leq 1\},$$
$$D_L = D \cap \{y = -1\},$$
$$D_S = D \cap \{x^2 + u^2 = (M\varepsilon)^2\},$$
$$D_R = D \cap \{y = 1\}.$$

Let E^3 denote $(v, w, y)-$phase space. The projection $\pi_y : E^3 \to E^1$ is given by $\pi_y(v, w, y) = y$. We define that $\phi : \mathbb{R}^3 \to E^3$ is a y-homeomorphism if ϕ is a homeomorphism and $\pi_y\phi(x_1, u_1, y_1) \leq \pi_y\phi(x_2, u_2, y_2)$ when $y_1 \leq y_2$.

3.3.1 The Steady Branch and its Dynamics.

The trajectories of the solutions near the steady branch S can be described as follows.

Proposition 1. *There exists $\varepsilon_S > 0$ and $M(\varepsilon_S) > 0$ such that for $0 < \varepsilon \leq \varepsilon_S$, there exists a y-homeomorphism $\phi_S : D \to E^3$ for which $N_S \equiv \phi_S(D)$ forms a neighborhood of the steady branch S with the following properties:*

a) $S \subset N_S$, and the Hopf bifurcation point y_H corresponds to $z = 0$ at the center of the tube D,

b) $N_S \subset M_- \equiv \{g < 0\}$,

c) $\pi_y(\phi_S(D_R)) = y_\rho$,

d) if $\gamma(t_0) \in \phi_S((\partial D \setminus D_R) \cap \{z > 0\})$ is on the boundary of N_S at $y = y_0 > y_H$, then $\gamma(t)$ enters and remains within N_S in forward time until it exits N_S with $y = y^0 < y_H$ at a time $T_1 + O(\varepsilon)$, where both y^0 and the time duration T_1 are functions of y_0.

To make the system 3.1 more manageable we introduce some change of variables.

We make the change of variables $\hat{x} = v - v_0(y)$, $\hat{u} = w - w_0(y)$, which translates the steady branch S to the origin of (FS) for each y, and then diagonalize the system, using $(\hat{x}, \hat{u}) = B(y, \varepsilon)(x, u)$. Near the steady branch, equation (2.1) thus becomes

$$x' = \xi_1(y)x + g_1(x, u, y) + \varepsilon h_1(y, \varepsilon), \tag{3.4a}$$

$$u' = \bar{\xi}_1(y)u + g_2(x, u, y) + \varepsilon h_2(y, \varepsilon), \tag{3.4b}$$

$$y' = \varepsilon g[(v_0(y), w_0(y)) + B(y, \varepsilon)(x, u), y] = -\varepsilon g_3(x, u, y, \varepsilon) \tag{3.4c}$$

where $B(y, \varepsilon)$ is a diagonalizing matrix , $u = \bar{x}$, $g_2 = \bar{g}_1$, and $h_2 = \bar{h}_1$, with

$$g_1 = O(\varepsilon)x + O(\varepsilon^2)u + O(|x|^2, |u|^2), \tag{3.5}$$

$$g_2 = O(\varepsilon)u + O(\varepsilon^2)x + O(|x|^2, |u|^2), \tag{3.6}$$

and $h_i = O(1)$. The different orders in equation (3.2) occur because when we diagonalize the right hand side of (3.1), a higher order off-diagonal term arises from differentiation of $B(y, \varepsilon)(x, u)$ with respect to y. For slow equation (3.1c), we have $0 < g_3 = g_4(y, \varepsilon) + o(|x| + |u|)$, which is positive when (x, u) is small by (H3). We introduce y as the new independent variable and change equation (3.1) into

$$\varepsilon x_y = -\lambda_1(y)x + \hat{G}_1(x, u, y) + \varepsilon H_1(y, \varepsilon), \tag{3.7a}$$

$$\varepsilon u_y = -\bar{\lambda}_1(y)u + \hat{G}_2(x, u, y) + \varepsilon H_2(y, \varepsilon). \tag{3.7b}$$

The higher order terms satisfy

$$\hat{G}_1 = O(\varepsilon)x + O(\varepsilon^2)u + O(|x|^2, |u|^2), \tag{3.8a}$$

$$\hat{G}_2 = O(\varepsilon)u + O(\varepsilon^2)x + O(|x|^2, |u|^2) \tag{3.8b}$$

and $H_i = O(1)$. By (H6), the eigenvalues satisfy $Re\lambda_j(y) < 0$ when $y > y_H$; $Re\lambda_j(y) > 0$ when $y < y_H$; and $Im\lambda_1(y_H) < 0$. Further, a transverse crossing occurs so that $-\frac{dRe\lambda_j(y)}{dy} = a_3 > 0$ at the Hopf bifurcation point $y = y_H$.

There are numerous discussions [2, 4, 5, 7, 6, 8, 9, 10, 18, 19, 23, 24, 25, 28, 34, 36, 37, 38, 39, 39] and [46, 47, 48, 50, 53, 29, 57, 59, 60, 61, 62, 63, 64, 64, 77, 80, 83, 86, 87, 88, 89, 90, 91] on the behavior of solutions to equation (3.7). Most of the previous work considers how y increase past y_H, while in our case, y decreases past y_H. We keep the minus sign in front of λ_1 in equation (3.7) to preserve the consistency of notation with other related works. We summarize some relevant results in the following theorem.

Theorem 5 ([60, 61, 86, 87])**.** *Let $(x, u)(y, \varepsilon)$ be any family of solutions of equations (3.7-3.8) with initial conditions that satisfy $|(x, u)(y_i, \varepsilon)| \leq M_1\varepsilon$ for $y_i > y_H$ and some $M_1 > 0$. Then there exist $M = M(M_1) > 0, y_q = y_q(M_1, M) < y_H, \varepsilon_S = \varepsilon_S(M_1, M)$ such that*

$$|(x, u)(y, \varepsilon)| \leq M\varepsilon$$

whenever $y_i \geq y \geq y_q, 0 \leq \varepsilon \leq \varepsilon_S$. Further, if y_i is close enough to y_H, then y_q and y_i satisfy the relationship

$$\int_{y_i}^{y_q} Re\lambda_1(\tau)d\tau = 0. \tag{3.9}$$

Remark 3.

The relation (3.9) holds for y_i close enough to y_H. When y_i is away from y_H, maximal delay phenomena [19] may occur in which y_q will no longer decrease as y_i increases. However, such complications do not occur in our situation.

Thus, we can simply choose $M_1 > 0$, find $M(M_1)$ and $\varepsilon_S(M, M_1)$ from Theorem 3.2, and for any $0 < \varepsilon \leq \varepsilon_S$ set $D = \{x^2 + u^2 \leq (M\varepsilon)^2, y_l \leq y \leq y_\rho\}$ where $y_l < y_H$ is the point satisfying

$$\int_{y_l}^{y_\rho} Re\lambda_1(\tau)d\tau = 0. \tag{3.10}$$

If (x, u, y) enters D at $y = y_0$, then it must exit D at $y = y^0$, where $y^0 < y_H$ is the point such that

$$\int_{y_0}^{y^0} Re\lambda_1(\tau)d\tau = 0. \tag{3.11}$$

The time duration can be calculated from the slow equation (3.4c),

$$\int_{y_0}^{y^0} \frac{1}{g(U_y, \varepsilon)}\, dy = \varepsilon T_1 + O(\varepsilon^2). \tag{3.12}$$

With these results in hand, the rest of the argument in Proposition 3.1 follows easily. In fact, there exists a y-diffeomorphism $\psi : D \to E^3$ such that under ψ, the slow equation has the canonical form

$$y' = -\varepsilon. \tag{3.13}$$

Remark 4.

Using Proposition 1, Equation (3.1) can be transformed into a homogeneous system for (X, U) (see [92]), namely

$$\varepsilon X_y = -\lambda_1(y)X + G_1(X, U, y, \varepsilon), \tag{3.14a}$$

$$\varepsilon U_y = -\bar{\lambda}_1(y)U + G_2(X, U, y, \varepsilon) \tag{3.14b}$$

where

$$G_1 = O(\varepsilon)X + O(\varepsilon^2)U + O(|X|^2, |U|^2), \tag{3.15a}$$

$$G_2 = O(\varepsilon)U + O(\varepsilon^2)X + O(|X|^2, |U|^2). \tag{3.15b}$$

Since $U = \bar{X}$, we write equation (3.10) in the complex form

$$\varepsilon X_y = -\lambda_1(y)X + G_1(X, \bar{X}, y, \varepsilon), \tag{3.16}$$

where G_1 has the form $G_1 = \varepsilon a(y, \varepsilon)X + O(\varepsilon^2)\bar{X} + O(X^2, X \cdot \bar{X}, \bar{X}^2)$ and equation (3.16) has an analytic extension into the complex plane z,

$$\varepsilon X_z = -\lambda_1(z)X(z) + G_1(X(z), \bar{X}(\bar{z}), z, \varepsilon), \tag{3.17}$$

where $\bar{X}(\bar{z})$ is the analytic extension for $\bar{X}(\bar{y})$. This will be important in Section 3.5.

3.3.2 The Periodic Branch and its Dynamics.

The behavior of solutions near a family of periodic orbits, terminating at one end in a Hopf bifurcation and at the other end in a homoclinic bifurcation, was discussed in detail by Terman [99, 100] (see also Rubin and Terman [72], and note that earlier results were obtained by Pontryagin and Rodygin ([67]), and we use similar ideas here.

Recall that each $P_y(t)$ is an asymptotically stable periodic solution. For each $y \in (y_h, y_r)$, we seek a compact neighborhood of $P_y(t)$ in $E^3 = (v, w, y)$ phase space. In particular, let

$$A = \{(x, u, y) : 1 - 2M\varepsilon \leq x^2 + u^2 \leq 1 + 2M\varepsilon, -1 \leq y \leq 1\},$$

$$A_R = \{(x, u, y) : 1 - 2M\varepsilon \leq x^2 + u^2 \leq 1 + 2M\varepsilon, y = 1\},$$

$$A_L = \{(x, u, y) : 1 - 2M\varepsilon \leq x^2 + u^2 \leq 1 + 2M\varepsilon, y = -1\},$$

$$A_S = \{(x, u, y) : x^2 + u^2 = 1 - 2M\varepsilon, \text{ or } x^2 + u^2 = 1 + 2M\varepsilon, \quad -1 \leq y \leq 1\}.$$

Proposition 2. *There exists $\varepsilon_P > 0$ and $M(\varepsilon_P) > 0$ such that for $0 < \varepsilon \leq \varepsilon_P$, there exists a y-homeomorphism $\phi_P : A \to E^3$ for which $N_P \equiv \phi_p(A)$ forms a neighborhood of the periodic branch P with the following properties:*

a) $P \subset N_P$ and the right knee of P at $y = y_r$ is at the right end of N_P corresponding to $z = 1$; that is, $\pi(\phi_P(A_R)) = y_r$,

b) $N_P \subset M_+ \equiv \{\hat{g} > 0\}$,

c) $\pi_y(\phi_P(A_L)) = y_\lambda$,

d) if $\gamma(t_0) \in \phi_P(\partial A \backslash A_R)$ is on the boundary of N_P at $y = y(t_0)$, then $\gamma(t)$ enters N_P in forward time and remains there until it exits at the right end $N_P \cap \{z = 1\}$ at time $T_2 + t_0 + O(\varepsilon)$, where the duration time T_2 is determined by the initial value $y(t_0)$.

The proposition follows from the stability properties of the periodic solutions of (FS). To apply the averaging method [75], we solve

$$V' = f_1(V, W, Y(t)), \tag{3.18a}$$

$$W' = f_2(V, W, Y(t)), \tag{3.18b}$$

$$Y' = \varepsilon \frac{1}{\tau(Y)} \int_0^{\tau(Y)} g(P_y(s), Y)\, ds \equiv \varepsilon \hat{g}(V, W, Y, \varepsilon), \tag{3.18c}$$

$$(V, W, Y)(t_0) = (v(t_0), w(t_0), y(t_0)) \tag{3.18d}$$

where $\tau(Y)$ is the period of the periodic solution $P_y(t)$ of (FS) with $y = Y$ and (v, w, y) denotes a solution to equation (3.1).

Remark 5.

Using Fenichel coordinates [27] with N_P, we find that the averaged equation (3.18) can be reduced to the canonical form

$$r' = -(r - 1), \tag{3.19a}$$

$$\theta' = c(y) > 0, \tag{3.19b}$$

$$y' = \varepsilon g_0(y) > 0. \tag{3.19c}$$

We shall use this form for the proofs below and for the study of the noisy case.

Remark 6.

The contraction behavior of solutions of equation (3.7) can be characterized by the following proposition; we will use a stochastic version of this in Section 3.5

Proposition 3. *Assume that* $(x,u)_A$ *and* $(x,u)_B$ *are two solutions of equation (3.7) on* $y_1 < y < y_2$, *and* $|(x,u)_A(y)| \le M_2\varepsilon$, $|(x,u)_B(y)| \le M_2\varepsilon$ *whenever* $y_1 \le y \le y_2$. *Then there exist* $M_3 = M_3(M_2) > 0$, $\varepsilon_0 = \varepsilon_0(M_2) > 0$ *so that for* $0 < \varepsilon \le \varepsilon_0$,

$$\frac{1}{M_3} e^{\frac{-1}{\varepsilon}\int_{y_1}^{y_2} Re\lambda_1(\tau)d\tau} \le \frac{|(x,u)_A(y_2) - (x,u)_B(y_2)|}{|(x,u)_A(y_1) - (x,u)_B(y_1)|} \le M_3 e^{\frac{-1}{\varepsilon}\int_{y_1}^{y_2} Re\lambda_1(\tau)d\tau}. \tag{3.20}$$

3.4 General Assumptions and Results on Noisy Elliptic Bursters.

We now turn to the effect of a random force to the elliptic bursters. We consider the system

$$dv = f_1(v,w,y)dt + \varepsilon^2\sigma\hat{h}_1(y)dW(y), \tag{3.21a}$$

$$dw = f_2(v,w,y)dt + \varepsilon^2\sigma\hat{h}_2(y)dW(y), \tag{3.21b}$$

$$dy = \varepsilon g(E_t(v), E_t(w), y)dt \tag{3.21c}$$

where $E_t(\cdot)$ is the expected value. The noisy term is modeled in similar terms by Baer et al. [5], Kuske [43] and Kuske and Baer [44]. The magnitudes $\hat{h}_i$ are assumed to be positive. The Brownian motions $W(y)$ are based on the usual hypotheses:

(1) $W(y_1) - W(y_2)$ is Gaussian $N(0, \sqrt{|y_1 - y_2|})$,

(2) $W(y_1) - W(y_2)$ and $W(y_3) - W(y_4)$ are independent if intervals which ended at y_1,y_2 and y_3, y_4 are disjoint.

In our problem, the variable y is deterministic. In a recent paper of Berglund and Gentz [8], a more general problem of noisy dynamic bifurcation with random slow passage was investigated. When the noise on y-equation is sufficiently small, the results are proven to be similar to those of deterministic slow passage.

The parameter σ is ranged from exponentially small at $O(e^{-\frac{C}{\varepsilon}})$ to $O(1)$ in this work.

We consider the dynamic behavior of the elliptic burster under such a noise. Particularly we are interested in the time durations T_1 on the steady branch and T_2 on the periodic branch. As typical for stochastic problems, we discuss problems in terms of large probability events below. We see that motions near the periodic branch are not affected much by the noise because the periodic orbits are attracting, although the time duration T_2 does depend on the y value where the trajectory enters N_P. A short T_1 will be followed a short T_2 and a longer T_1 will be followed by a longer T_2. In brief, T_1 largely determines T_2, as we will show below. The duration T_1 spent inside N_S (i.e., the effect of noise on delayed bifurcation) is therefore a key to understanding the patterns of the elliptic burster.

We note here that the ratio of noise amplitude versus passage speed is quite crucial to our problem. As indicated by Weinberger and Rosenblat [106], if the ratio is large, then the dynamics is overwhelmed by noise, there could be advance in bifurcation rather than delay. For smaller ratio, situations are still very delicate, as observed in noisy dynamic pitchfork bifurcation [7, 83, 95]. Dynamics is different when the ratio changes from exponentially small to polynomially small.

We study the time duration T_1 through a geometric analysis for the distribution of the jumping point Y_j where the solution exits N_S and heads for N_P. For technical reason, we redefine N_S to be $\varepsilon^{1+\gamma}, 0 < \gamma < 1/4$ neighborhood of S.

We define the jump point Y_j to be the first exit point from N_S:

$$Y_j(\omega) = \sup_{y \le y_r} \{y | X(y, \omega) \in \partial N_S\}$$

i.e., $X(Y_j, \omega) \in \partial N_S$ and $X(y, \omega) \in N_S$ for $Y_j < y \le y_r$. We drop ω in the text below for simplicity.

Theorem 6 (Main Theorem. Su, Rubin Terman)**.** *There exists ε_0 such that for $0 < \varepsilon \le \varepsilon_0$, equation (3.21) possesses bursting solutions for which the loop time $T_\varepsilon(t)$ satisfies the relation $T_\varepsilon(t) = T_1 + T_2 + o(1/\varepsilon)$, where T_1, T_2 are the times spent inside N_S near the steady state curve S and inside N_P near the periodic orbit family P, respectively. With the exception of some small probability events noted below in Remark 4.2, the random variables $T_i, i = 1, 2$ are determined by the jump point Y_j (first exit time from N_S) through the relations:*

$$\int_{y_r}^{Y_j} \frac{1}{g(U(y),\varepsilon)}\, dy = \varepsilon T_1 + O(\varepsilon^2) \tag{3.22}$$

and

$$\int_{Y_j}^{y_r} \frac{\tau(y)}{\int_0^{\tau(y)} g(P_y(s), y)\, ds}\, dy = \varepsilon T_2 + O(\varepsilon^2). \tag{3.23}$$

The jumping point Y_j is a random variable, related to a complex distance function Δ defined as: $\Delta(y) = \varepsilon\sigma\int_{y_r}^{y} \hat{H}(s) e^{\frac{-1}{\varepsilon}\int_s^y \lambda_1(\tau) - \varepsilon a(\tau,\varepsilon) + O(\varepsilon^{1+\gamma}) d\tau} dW(s)$ where $\hat{H}(s)$ is the noise variation to be defined in Equation (3.24) below. The "average" jumping point $\bar{Y}_j < y_H$ satisfies the formula

$$\int_{y_H}^{\bar{Y}_j} Re\lambda_1(y) + O(\varepsilon)\ dy = -\varepsilon(\ln M\varepsilon^{\gamma-\frac{1}{4}}/\sigma) = \varepsilon \ln\sigma + O(\varepsilon|\ln\varepsilon|).$$

Further there exist $K_0 = K_0(\varepsilon_0) > 0$, $C_0 = C_0(\varepsilon_0) > 0$ such that for $K \ge K_0, \varepsilon \le \varepsilon_0$, for cases where $\bar{Y}_j = y_H - O(1)$,

$$Prob(|Y_j - \bar{Y}_j| \ge K\varepsilon) \le e^{-C_0 K}.$$

But for cases where $\bar{Y}_j$ is very near y_H, say $Y_j = y_H - O(\sqrt{\varepsilon \ln \varepsilon})$, the deviation is of order $\sqrt{K\varepsilon}$ and the estimate is revised as

$$Prob(|Y_j - \bar{Y}_j| \geq \sqrt{K\varepsilon}) \leq e^{-C_0 K}.$$

The jumping points are clustered together near $\bar{Y}_j$. Therefore, only when $\sigma \leq O(e^{-C/\varepsilon})$ for large enough C there is a regular pattern of long bursts. When $O(1) \geq \sigma \geq O(\varepsilon^n), n \in \mathbb{N}$, there is a pattern of short bursts with a very small probability of long bursts. When σ falls in range between $O(e^{-C/\varepsilon})$ and $O(\varepsilon^n)$, there is a distribution of bursts of different lengths.

Remark 7.

To be more specific, when $\sigma \geq O(\varepsilon^n), n \in \mathbb{N}$, the exit points from N_S are $Y_j \sim \bar{Y}_j = y_H - O(\sqrt{\varepsilon |\ln(\varepsilon)|})$, located very near the bifurcation point y_H, and we see a short period of large spikes in active phase as well as a short period of small oscillations in silent phase. When $\sigma \leq O(e^{-C/\varepsilon})$, $Y_j \sim \bar{Y}_j = y_H - O(1)$, and longer periods in each phase are exhibited. See Figures 3.3a and 3.3b.

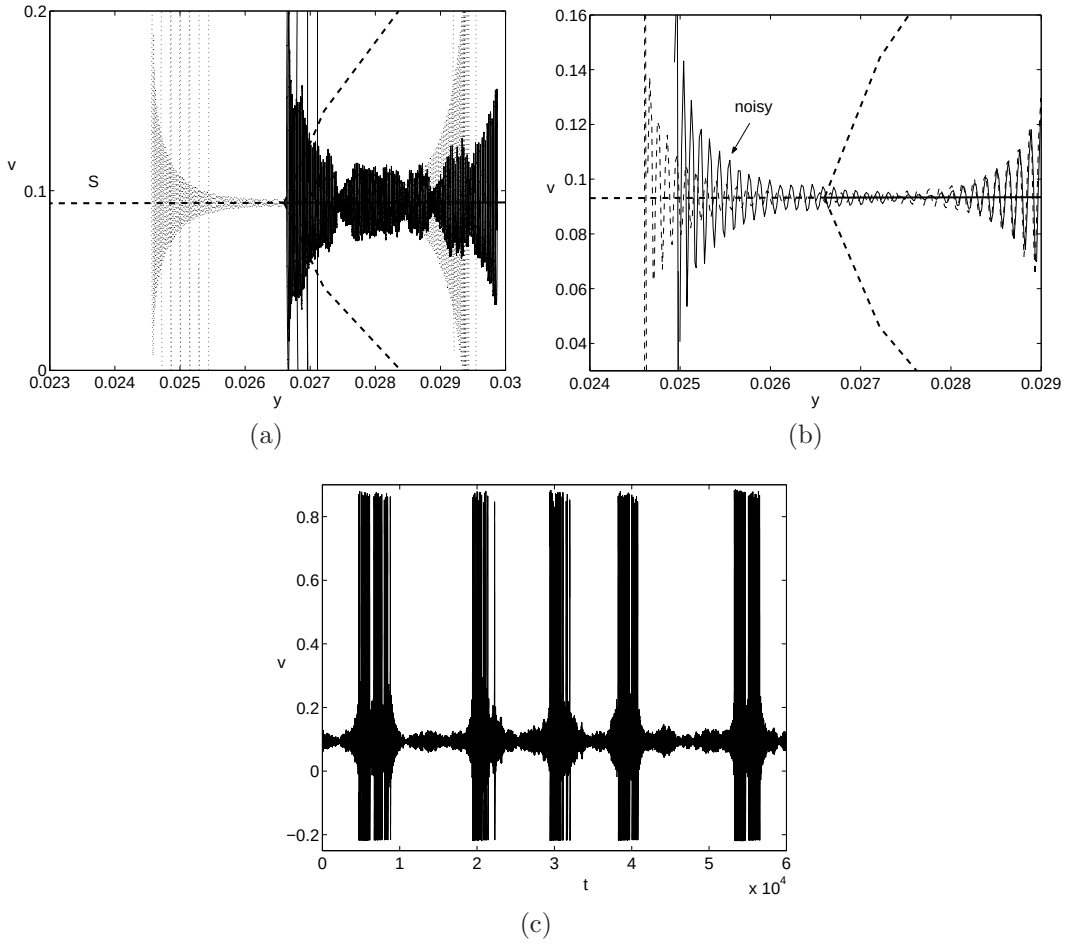

Figure 3.3: (a). Short duration noisy delay when $\sigma = O(\varepsilon^n)$. The solid curve shows a trajectory that jumps up extremely close to y_H with noise $\delta = \varepsilon = .0005$ in the Wu-Baer model, while the dotted curve shows a deterministic trajectory for the same parameter values. The dashed curves are the bifurcation curves for (FS); note that this figure is zoomed in, in the neighborhood of y_H, relative to Figures 1 and 2 (b) Long duration noisy delay when $\sigma = O(\varepsilon^{-\frac{c}{\varepsilon}})$. The solid curve shows a trajectory that has a long duration noisy delay beyond y_H with noise $\delta = 5 \times 10^{-5}$ and $\varepsilon = .0005$ in the Wu-Baer model, while the dotted curve shows a deterministic trajectory for the same parameter values for comparison. The dashed curves are the bifurcation curves for (FS); The equations were solved with Euler's method with a time step of $dt = .02$; the values of (v, y) were plotted once every 3000 time steps for this figure and (c) A mixture of long and short delays and burstings. The curve, a trajectory in v versus t, has a mixture of long and short times in N_S for the Wu-Baer model with $\varepsilon = .0005$, noise $\delta = .00075$. The equations were solved with Euler's method with a time step of $dt = .05$; the values of (v, y) were plotted once every 5 time steps for this figure

For the values of σ in between $O(e^{-C/\varepsilon})$ and $O(\varepsilon^n)$, the mixed patterns of different phase lengths are related to a random complex distance whose distribution is nearly Gaussian, as illustrated in Figure 4c. Note that we write $-O(\ldots)$ here to emphasize the fact that the jump out of N_S occurs after y drops below y_H, in all cases. In the statement of the Theorem and in the proof below, we use the conventional notation and write $+O(\ldots)$, even when we know that the higher order terms are negative.

Remark 8.

The event that equations (3.22) and (3.23) hold is of large probability. There are small probability events, namely that the trajectories could exit the neighborhood N_S and then come back, that are not considered in equation (3.22); similarly, trajectories could with small probability exit earlier out of N_P than indicated by equation (3.23). In a similar analysis of Burgland and Gentz [7] for a one dimensional real system, it was shown that such occurrence is of exponentially small probability when the amplitude of noise is small.

Remark 9.

Our estimate of $\bar{Y}_j$ is consistent with earlier results in [4,52,59] after rescaling, since our method is applicable to pitchfork bifurcation as well. Detail will be provided in Section 3.5.

3.5 Analysis of Noisy Delayed Bifurcations and Elliptic Bursters

We use the same linear transformations used to derive equation (3.16) from equation (3.1) to transform the equation (3.21) into a system

$$\varepsilon dX = [-\lambda_1(y)X + G_1(X, \bar{X}, y)]dy + \varepsilon^2 \sigma \hat{H}(y) dW, \tag{3.24}$$

where G_1 has the expression $G_1 = \varepsilon a(y,\varepsilon)X + O(\varepsilon^2)\bar{X} + O(X^2, X\cdot\bar{X}, \bar{X}^2)$.

We note here Equation (3.24) is derived through a linear transformation. When nonlinear transformation is used to derive these canonical form such as equation (3.19), there will be an additional term of order $\varepsilon^4\sigma^2$ due to Ito's Lemma. However, these terms are too small to cause any harm.

We need some technical lemmas to start, proceeding initially in analogy to the treatment of the deterministic case in [86, 87]. We see that the exponential growth property, specified in Proposition 3.4, remains valid in this stochastic case.

Proposition 4. *Assume that X_A and X_B are two solutions of (3.24) on $y_1 < y < y_2$. Given the event $\Omega_1 = \{\omega || X_A(y)(\omega)| \le M_2\varepsilon, |X_B(y)(\omega)| \le M_2\varepsilon\}$ for some $M_2, \varepsilon > 0$ whenever $y_1 \le y \le y_2$. Then there exist $M_3 = M_3(M_2)$, $\varepsilon_0 = \varepsilon_0(M_2)$ so that for $\varepsilon \le \varepsilon_0$,*

$$\frac{1}{M_3} e^{\frac{-1}{\varepsilon}\int_{y_1}^{y_2} Re\lambda_1(\tau)d\tau} \le \frac{|X_A(y_2)(\omega) - X_B(y_2)(\omega)|}{|X_A(y_1)(\omega) - X_B(y_1)(\omega)|} \le M_3 e^{\frac{-1}{\varepsilon}\int_{y_1}^{y_2} Re\lambda_1(\tau)d\tau}, \omega \in \Omega_1. \quad (3.25)$$

Proof We consider that $X = X_A(y)(\omega) - X_B(y)(\omega)$ satisfies a deterministic equation similar to equation 3.12, since the noise is additive. This result follows similarly to the deterministic case because $|X_A(y)(\omega)| \le M_2\varepsilon$, $|X_B(y)(\omega)| \le M_2\varepsilon$.

Lemma 1. *Assume transversal eigenvalue crossing at the Hopf bifurcation, stated by (H6) in Section 2. Let*

$$\xi(y) \equiv \int_y^{y_r} |\hat{H}(s)|^2 e^{\frac{-2}{\varepsilon}\int_s^y Re(\lambda_1(\tau) - \varepsilon a(\tau,\varepsilon))d\tau} ds. \quad (3.26)$$

Assume $|\hat{H}(y)| \neq 0$. There exist C_1, C_2 and ε_0 such that when $\varepsilon \le \varepsilon_0$,

$$C_1\sqrt{\varepsilon} \le \xi(y) \le C_2\sqrt{\varepsilon}, \qquad y_H - \sqrt{\varepsilon} \le y \le y_r \quad (3.27)$$

and

$$C_1\sqrt{\varepsilon}e^{\frac{-2}{\varepsilon}\int_{y_H}^{y} Re(\lambda_1(\tau)-\varepsilon a(\tau,\varepsilon))d\tau} \leq \xi(y) \leq C_2\sqrt{\varepsilon}e^{\frac{-2}{\varepsilon}\int_{y_H}^{y} Re(\lambda_1(\tau)-\varepsilon a(\tau,\varepsilon))d\tau}, \qquad y_l \leq y \leq y_H-\sqrt{\varepsilon}. \tag{3.28}$$

The condition $|\hat{H}(y)| \neq 0$ *can be relaxed to that* $\dfrac{\partial^j(|\hat{H}(y)|^2)}{\partial y^j} = 0, j = 0, 1, \cdots, n-1$ *but* $\dfrac{\partial^n(|\hat{H}(y)|^2)}{\partial y^n} \neq 0$. *Then the left hand sides of the inequalities (3.27- -3.28) should be revised to*

$$C_1\sqrt{\varepsilon}\varepsilon^n \leq \xi(y) \leq C_2\sqrt{\varepsilon}, y_H - \sqrt{\varepsilon} \leq y \leq y_r \tag{3.29}$$

and

$$C_1\sqrt{\varepsilon}\varepsilon^n e^{\frac{-2}{\varepsilon}\int_{y_H}^{y} Re(\lambda_1(\tau)-\varepsilon a(\tau,\varepsilon))d\tau} \leq \xi(y) \leq C_2\sqrt{\varepsilon}e^{\frac{-2}{\varepsilon}\int_{y_H}^{y} Re(\lambda_1(\tau)-\varepsilon a(\tau,\varepsilon))d\tau}, y_l \leq y \leq y_H-\sqrt{\varepsilon}. \tag{3.30}$$

Proof If $c_1 \leq |\hat{H}(y)| \leq c_2$, then

$$\int_y^{y_r} c_1^2 e^{\frac{-2}{\varepsilon}\int_s^y Re(\lambda_1(\tau)-\varepsilon a(\tau,\varepsilon))d\tau} ds \leq \xi(y) \leq \int_y^{y_r} c_2^2 e^{\frac{-2}{\varepsilon}\int_s^y Re(\lambda_1(\tau)-\varepsilon a(\tau,\varepsilon))d\tau} ds.$$

Lemma 1 follows directly from Lemma 4.2 of [7] with exception of the special case. When it happens, we notice $|\hat{H}(y+\varepsilon)| \geq M_4\varepsilon^n$ and the integrand is positive. Then

$$\xi(y) \geq \int_{y+\varepsilon}^{y_r} |\hat{H}(s)|^2 e^{\frac{-2}{\varepsilon}\int_s^y Re(\lambda_1(\tau)-\varepsilon a(\tau,\varepsilon))d\tau} ds \tag{3.31}$$

implies Equation 3.29-3.30 by the same analysis above.

Proof of Theorem 6 The existence of solution for was considered in [40, 42, 45]. Here we concentrate on the behavior of $X(y)$ within N_S.

From Lemma 1, the contraction property of the solutions, it is only necessary to consider $X_0(y)$, the solution of equation (3.24) with the initial condition $X_0(y_r) = 0$.

Further, since we are only interested the first exit time Y_j, we modify the nonlinearity in equation (3.24) as follows:

$$\varepsilon dX = [-(\lambda_1(y) - \varepsilon a(y,\varepsilon))X + G_2(X,\bar{X},y)X]dy + \varepsilon^2\sigma\hat{H}(y)dW$$

where G_2 has the expression $G_2 = O(\varepsilon^2)(\bar{X})/X + O(X^2, X\cdot\bar{X}, \bar{X}^2)/X$. We define a smooth function $G(X)$ such that $G = G_2$ when $|X| \leq M\varepsilon^{1+\gamma}$ and $G = 0$ when $|X| \geq 2M\varepsilon^{1+\gamma}$. Then $\sup_{X\in\mathbb{C}} |G(X)| \leq O(\varepsilon^{1+\gamma})$. The new equation

$$\varepsilon dX = [-(\lambda_1(y) - \varepsilon a(y,\varepsilon))X + G(X)X]dy + \varepsilon^2\sigma\hat{H}(y)dW, \tag{3.32}$$

is equivalent to Equation (3.24) for any trajectory $X(y) \in N_S$, therefore it determines the same distribution for Y_j. We analyze equation (3.32) instead.

Since $X_0(y_r) = 0$, we compute directly the distance from $X_0(y)$ to the origin of the complex plane for $y_l \leq y \leq y_r$ by solving equation (3.32) directly:

$$\Delta(y) = X_0(y) = \varepsilon\sigma\int_{y_r}^{y} \hat{H}(s)e^{\frac{-1}{\varepsilon}\int_s^y(\lambda_1(\tau)-\varepsilon a(\tau,\varepsilon)-G(X))d\tau}dW(s)$$

$$= \varepsilon\sigma\int_{y_r}^{y} \hat{H}(s)e^{\frac{-1}{\varepsilon}\int_s^y(\lambda_1(\tau)-\varepsilon a(\tau,\varepsilon))d\tau}(1+O(\varepsilon^\gamma))dW(s) \;= \Delta_1 + \Delta_2 \tag{3.33}$$

where

$$\Delta_1 = \varepsilon\sigma\int_{y_r}^{y} \hat{H}(s)e^{\frac{-1}{\varepsilon}\int_s^y(\lambda_1(\tau)-\varepsilon a(y,\varepsilon))d\tau}dW(s) \tag{3.34}$$

is Gaussian. We calculate the mean and variance of Δ_1 and Δ_2:

$$E(\Delta_1) = \varepsilon\sigma\int_{y_r}^{y} \hat{H}(s)e^{\frac{-1}{\varepsilon}\int_s^y(\lambda_1(\tau)-\varepsilon a(\tau,\varepsilon))d\tau}E(dW(s)) = 0. \tag{3.35}$$

Then for $y_H - \sqrt{\varepsilon} \leq y \leq y_r$,

$$E(\Delta_2) = \sigma | \int_{y_r}^{y} \hat{H}(s) e^{\frac{-1}{\varepsilon}\int_s^y (\lambda_1(\tau) - \varepsilon a(\tau,\varepsilon))d\tau} E(O(\varepsilon^{1+\gamma}) dW(s)) |$$

$$\leq O(\varepsilon^{1+\gamma}) \sigma \sqrt{\xi(y)} = O(\varepsilon^{\gamma+5/4})\sigma, \tag{3.36}$$

while for $y_l \leq y \leq y_H - \sqrt{\varepsilon}$,

$$E(\Delta_2) = \sigma | \int_{y_r}^{y} \hat{H}(s) e^{\frac{-1}{\varepsilon}\int_s^y (\lambda_1(\tau) - \varepsilon a(\tau,\varepsilon))d\tau} E(O(\varepsilon^{1+\gamma}) dW(s)) |$$

$$\leq O(\varepsilon^{1+\gamma}) \sigma \sqrt{\xi(y)} = O(\varepsilon^{\gamma+5/4})\sigma e^{\frac{-1}{\varepsilon}\int_{y_H}^{y} Re(\lambda_1(\tau) - \varepsilon a(\tau,\varepsilon)))d\tau}. \tag{3.37}$$

The inequalities (3.36-3.37) use the Ito's lemma [40] and Lemma 1 and are actually consequences of Equations (3.38-3.39) below.

In fact it is more significant to calculate the variable $|\Delta|^2$ since Y_j is determined by $|\Delta|^2(\omega) = M^2 \varepsilon^{2+2\gamma}$. From Ito's lemma [40], derived from the properties of Brownian motion as stated in hypotheses (1), (2) in Section 3.4, we get

$$\begin{aligned}
&E(\Delta_1 \bar{\Delta}_1) = \\
&\varepsilon^2 \sigma^2 E \left(\int_{y_r}^{y} \hat{H}(s) e^{\frac{-1}{\varepsilon}\int_s^y (\lambda_1(\tau) - \varepsilon a(\tau,\varepsilon))d\tau} dW(s) \overline{\int_{y_r}^{y} \hat{H}(s) e^{\frac{-1}{\varepsilon}\int_s^y (\lambda_1(\tau) - \varepsilon a(\tau,\varepsilon))d\tau} dW(s)} \right) \\
&= \varepsilon^2 \sigma^2 \int_{y}^{y_r} |\hat{H}(s) e^{\frac{-1}{\varepsilon}\int_s^y (\lambda_1(\tau) - \varepsilon a(\tau,\varepsilon))d\tau}|^2 ds \\
&= \varepsilon^2 \sigma^2 \int_{y}^{y_r} |\hat{H}(s)|^2 e^{\frac{-1}{\varepsilon}\int_s^y (2Re\lambda_1(\tau) - 2\varepsilon a(\tau,\varepsilon))d\tau} ds = \varepsilon^2 \sigma^2 \xi(y).
\end{aligned} \tag{3.38}$$

Similarly, we derive

$$
\begin{aligned}
&E(\Delta_2\bar{\Delta}_2) = \\
&\sigma^2 E\left(\int_{y_r}^{y} \hat{H}(s)e^{\frac{-1}{\varepsilon}\int_s^y(\lambda_1(\tau)-\varepsilon a(\tau,\varepsilon))d\tau}O(\varepsilon^{1+\gamma})dW(s)\right. \\
&\left.\cdot\overline{\int_{y_r}^{y} \hat{H}(s)e^{\frac{-1}{\varepsilon}\int_s^y(\lambda_1(\tau)-\varepsilon a(\tau,\varepsilon))d\tau}O(\varepsilon^{1+\gamma})dW(s)}\right) \\
&= O(\varepsilon^{2+2\gamma})\sigma^2\int_y^{y_r}|\hat{H}(s)|^2e^{\frac{-1}{\varepsilon}\int_s^y(2Re\lambda_1(\tau)-2\varepsilon a(\tau,\varepsilon))d\tau}ds = O(\varepsilon^{2+2\gamma})\sigma^2\xi(y).
\end{aligned}
\tag{3.39}
$$

Therefore, when $\varepsilon \le \varepsilon_0$,

$$C_3\varepsilon^2\sigma^2\xi(y) < E(\Delta(y)\bar{\Delta}(y)) < C_4\varepsilon^2\sigma^2\xi(y).$$

Following from Lemma 1, we have

$$C_1\sqrt{\varepsilon}C_3\varepsilon^2\sigma^2 \le E(\Delta(y)\bar{\Delta}(y)) \le C_2\sqrt{\varepsilon}C_3\varepsilon^2\sigma^2, \qquad y_H-\sqrt{\varepsilon} \le y \le y_r \tag{3.40}$$

and

$$
\begin{aligned}
&C_1C_3\varepsilon^{5/2}\sigma^2e^{\frac{-2}{\varepsilon}\int_{y_H}^{y}Re(\lambda_1(\tau)-\varepsilon a(\tau,\varepsilon))d\tau} \le E(\Delta(y)\bar{\Delta}(y)) \\
&\le C_2C_3\varepsilon^{5/2}\sigma^2e^{\frac{-2}{\varepsilon}\int_{y_H}^{y}Re(\lambda_1(\tau)-\varepsilon a(\tau,\varepsilon))d\tau}, \qquad y_l \le y \le y_H-\sqrt{\varepsilon}.
\end{aligned}
\tag{3.41}
$$

We define an "average" jumping point $\bar{Y}_j$ to be

$$E(|\Delta|^2(\bar{Y}_j)) = M^2\varepsilon^{2+2\gamma}. \tag{3.42}$$

From Equation. (3.40), we derive $\bar{Y}_j \le y_H-\sqrt{\varepsilon}$ since $\gamma < 1/4$. Now we solve the equation

$$\varepsilon^{\frac{5}{2}}\sigma^2e^{\frac{-2}{\varepsilon}\int_{y_H}^{y}Re(\lambda_1(\tau)-\varepsilon a(\tau,\varepsilon))d\tau} = M^2\varepsilon^{2+2\gamma}$$

to derive

$$-\int_{y_H}^{y} Re(\lambda_1(\tau) - \varepsilon a(\tau,\varepsilon))d\tau = \varepsilon \ln(M_4 \varepsilon^{\gamma-\frac{1}{4}}/\sigma), \tag{3.43}$$

then we have the expression of $\bar{Y_j}$.

The rest of Theorem 6 follows easily. Beyond the exceptional cases, the time duration T_1 is obtained as the time of passage inside N_S from $y = y_r$ down to $y = Y_j$, under the flow of the slow equation (3.21c).

$$|E_t(v,w) - (V_0(s), W_0(s))| \leq \sqrt{E_t|(v,w) - (V_0(s), W_0(s))|^2} \leq CE|X|^2 \leq M^2\varepsilon^{2+2\gamma}.$$

This yields equation (3.22).

When $\sigma = O(\varepsilon^n)$, the amount of delay will be $O(\sqrt{\varepsilon|\ln\varepsilon|})$, with a very small probability to have a significant $O(1)$ size delay. When $\sigma = O(e^{-\frac{C}{\varepsilon}})$, the delay will be significant almost surely.

For the values in between, there will be nontrivial distributions of different amount of delays which are responsible for different patterns. Let us assume σ is in that range, and $\varepsilon \ln \sigma$ is sufficient small. Then Equation 3.43 is approximated by

$$\frac{1}{2} Re\lambda_1'(y_H)(y - y_H)^2 + O((y - y_H)^3) = \varepsilon \ln(M_4 \varepsilon^{\gamma-\frac{1}{4}}/\sigma).$$

This implies

$$\bar{Y_i} = y_H - O(\sqrt{\varepsilon|\ln(\varepsilon^{\gamma-\frac{1}{4}})/\sigma|}). \tag{3.44}$$

Equation (3.44) is consistent with well known results from [7, 83, 95] after rescaling. Their amplitude of noise is equal to $\sigma\varepsilon^{3/2}$ in our notation, and N_S is also slightly different.

Remark 10.

The treatment here is quite general and the analysis and result are valid both for delayed simple eigenvalue bifurcations as well as for delayed Hopf bifurcations, since the imaginary part of the eigenvalue $\lambda_1(y)$ is not contributing here. For the noisy dynamic pitchfork bifurcation, a more precise description of Y_j in terms of its probability distribution was already given in [7].

The situation with the periodic branch is simpler due to the fact the periodic solutions of FS are orbitally stable. By using the Fenichel coordinates [27] and the invariant manifold argument in [6], equation (3.21) inside N_P can be reduced to a perturbation to equation (3.19),

$$dr = -(r-1)dt + \varepsilon^2 \hat{h}_3(y,\varepsilon)dW(y) + O(\varepsilon^4\sigma^2)dt, \tag{3.45a}$$

$$d\theta = c(y)dt + \varepsilon^2 \hat{h}_4(y,\varepsilon)dW(y) + O(\varepsilon^4\sigma^2)dt, \tag{3.45b}$$

$$y' = \varepsilon g_0(y) > 0. \tag{3.45c}$$

The additional terms at the end of Equation 3.45 are due to Ito's lemma applying to the nonlinear transformation here.

We can show easily that the solution $(R,\Theta,Y)(t)$ of the stochastic equation (3.45) and the solution $(r,\theta,y)(t)$ of equation (3.19), with the same initial condition at $t = t_0$, satisfy the relations

$$E(R,\Theta,Y) = (r,\theta,y), \tag{3.46}$$

and

$$E|(R,\Theta,Y) - (r,\theta,y)|^2 = O(\varepsilon^2). \tag{3.47}$$

Thus the solutions (R, Θ, Y) will remain within N_P and only exit when $y = y_r + O(\varepsilon|\ln\varepsilon|)$, the same as for (r, θ, y) with a certain exceptions noted in Remark **??**. Therefore the time duration T_2 is obtained as the passage time from $y = Y_j$ to $y = y_r$ inside N_P, using the slow motion for the averaged form of system (3.45). But by construction, this is equivalent to the passage time computed from the averaged form of system (3.21), which yields (3.23). Finally, the passages from N_S to N_P and from N_P to N_S are to leading order identical to the deterministic case.

Corollary 1. *Any solution (v, w, y) of equation (3.21) with its initial position in N_P or N_S is an elliptic bursting solution as described in Theorem 6.*

Proof If $(v(0), w(0), y(0)) \in N_P$, then the corresponding solution $(v(t), w(t), y(t))$ of (3.21) enters N_S. Thus, without loss of generality, let the complex solution $X(y)$ correspond to (v, w, y), a solution of (3.21) with $(v(0), w(0), y(0)) \in N_S$. The point where the solution $X(y)$ will exit N_S is determined by the distance function

$$\Delta_3 = X(y) = X(y) - X_0(y) + X_0(y) = X(y) - X_0(y) + \Delta. \tag{3.48}$$

Now, by Proposition 4 and in particular equation (3.25), there exists a constant $M > 0$ such that

$$|X(y) - X_0(y)| \leq M|X(y_r) - X_0(y_r)|e^{\frac{-1}{\varepsilon}\int_{y_r}^{y} Re\lambda_1(\tau)d\tau} \leq M\varepsilon(e^{-\frac{C}{\varepsilon}})$$

if $y_l < y$.

we derive

$$\Delta_2 = \Delta + O(\varepsilon e^{-\frac{C}{\varepsilon}}). \tag{3.49}$$

The jumping point Y_j for any solution will the same one as in Theorem 6, up to a $O(\varepsilon|\ln\varepsilon|)$ error.

3.6 Reliability of Spike Timing

When considering the similarity in the firing pattern of two elliptic bursters we need to take into account two phenomena. One is the similarity in the bursting pattern (see Figure 3.5) and the other is the similarity in the spiking pattern which is the object of this part.

3.6.1 Basic Tools

The present section shows some simulations of an elliptic burster. We want to determine directly the temporal precision with which it is capable to reproduce its bursting pattern in presence of noise. In order to do this we use Insterspike Interval Histograms (ISI) and Post-stimulus Time Histograms (PSTH). They were introduced by Gerstein and Kiang [30] to analyze quantitatively electrophysiological data from single neurons.

If the spikes in a train occur at times $t_i, (0 \leq i \leq N)$, then ISIs will be $\Delta t_i = t_i - t_{i-1}$ for $1 \leq i \leq N$. A standard method of measuring variability of a spike train is by the coefficient of variation of the interspike interval (ISIs), C_v. The irregularity of the spike train can be measured by the relative width C_v of the ISI distribution $\frac{C_v}{\overline{\Delta t}}$, where $\overline{\Delta t}$ is the mean of the ISI (see [35]). Random spikes yield values of C_v near 1 and regular spikes yield values near zero.

To measure how the firing pattern changes when it is perturbed by noise, the PSTH is used. We can visualize the rate and timing of neuronal spike discharges in relation to the instant of the most previous presentation of the stimulus, summed over many repeated stimulus presentations [30]. It is a standard tool in neurophysiology. An algorithm to choose the width of the intervals to group the data (bin) and build a PSHT is described in [79] (see Appendix B). Following [52] and [65] we define the reliability of the spiking in the following way:

Event. Given a threshold $\alpha > 0$, an event corresponds to bin(s) in the PSTH larger than α. This might be widened to include the bins immediately adjacent to these [65].

Reliability. The reliability is the cumulative sum of the bins in the PSTH that are larger than the threshold, divided by the the cumulative sum of all the bins.

The reliability is a measure of the probability of observing an action potential within the bins over the threshold.

3.6.2 Reliability

We solved the system of ODE's (3.50) which satisfies the hypothesis for elliptic bursters stated at beginning of this chapter. The quantity $\varepsilon^2 * sig * xi$ is the noise term, here xi is a variable that represents a Wiener process and sig controls the amplitude of the noise. To generate the spike trains we considered only the peaks above the threshold of -10mV, basically those peaks in the active phase. We can see the solution to the noiseless case $sig = 0$ in Figure 3.4.

$$
\begin{aligned}
v' &= -(gca * m_\infty(v) * (v - vca) + gk * w * (v - vk) + ... \\
&... + gl * (v - vl) + gkca * z(y) * (v - vk)) + I + \varepsilon^2 * sig * xi \\
w' &= phi * (w_\infty(v) - w)/tau(v) + \varepsilon^2 * sig * xi \\
y' &= \varepsilon(-mu * gca * m_\infty(v) * (v - vca) - y) \\
m_\infty(v) &= 0.5 * (1 + \tanh((v + 1.2)/18)) \\
w_\infty(v) &= 0.5 * (1 + \tanh((v - 2)/30)) \\
z(y) &= y/(1 + y) \\
\tau(v) &= \cosh((v - 2)/60)
\end{aligned}
\tag{3.50}
$$

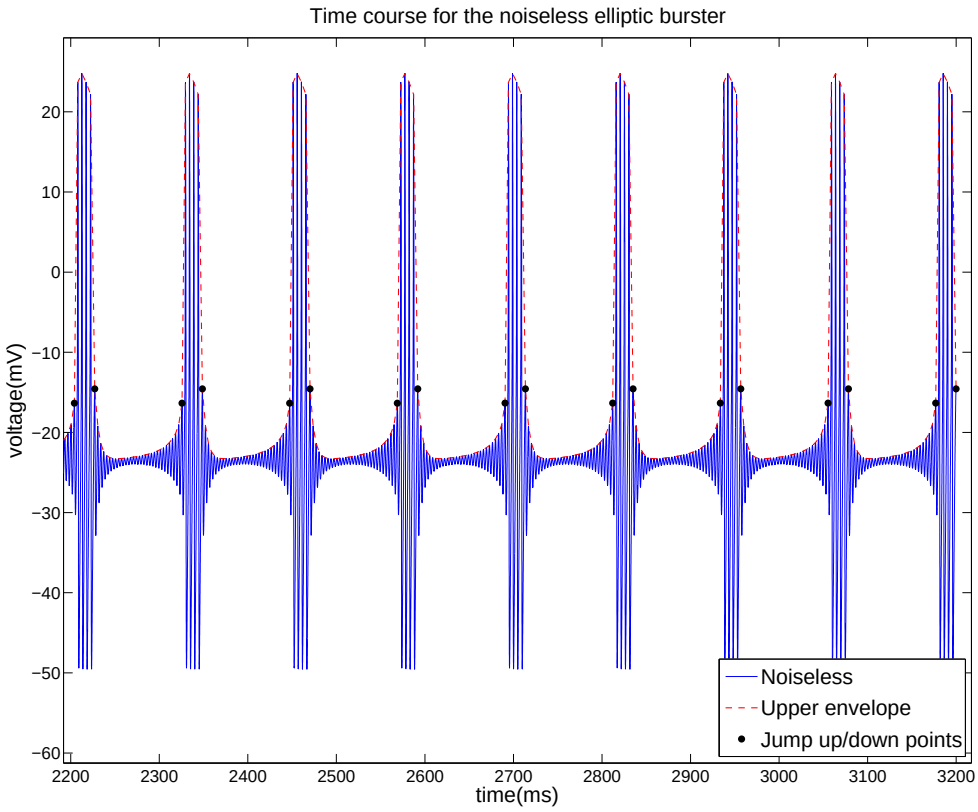

Figure 3.4: Solution of (3.50) with parameters $gca = 4.4$, $gk = 8$, $gl = 2vk = -84$, $vl = -60$, $vca = 120$, $I = 120$, $gkca = .75$, $phi = 1.2$, $\varepsilon = .04$, $mu = .016667$ $sig = 0$

We solved the system using XPPAUT (Euler method) with 100 seeds for the random number generator for each system with identical initial conditions and different levels of noise. Then we build the Post Stimulus Histograms (some of then can be seen in Figure 3.7). We use them to compute the reliability for different noise levels. The graph of Reliability versus Noise Level (Figure 3.8) shows that when we increase the noise level the reliability decrease in average but it does not do it monotonically. We also computed the C_v's yielding high values. It shows irregularity of the firing

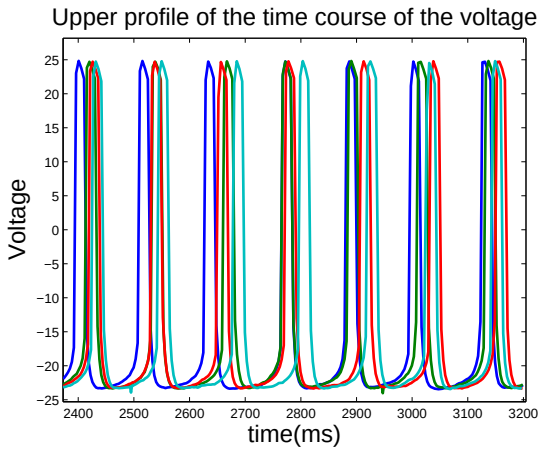

Figure 3.5: Upper envelope of the solution to system 3.50 with different types of noise and parameters as in Figure 3.4. $sig = 0.1$.

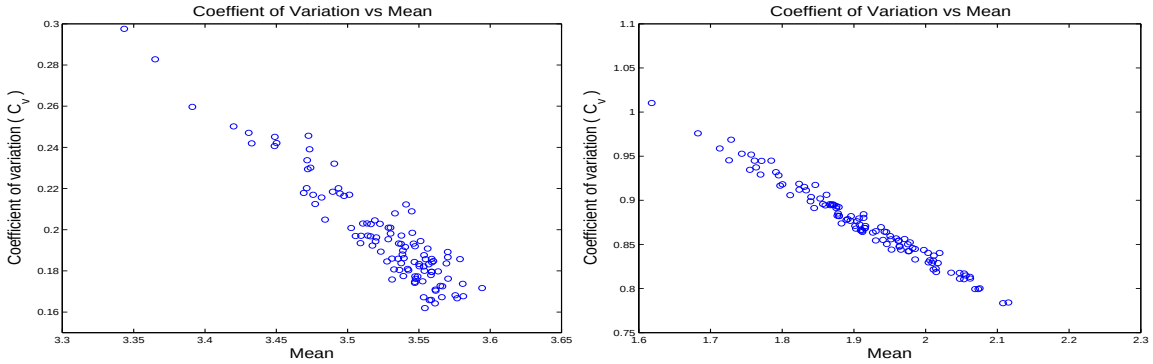

(a) (b)

Figure 3.6: C_v for single elliptic bursters. (a) Noise level 0.1. (b) Noise level 0.9

pattern in single neurons. As expected, the irregularity increases as noise increases. A scatter plot of C_v vs the mean of ISI's for two noise levels is shown in Figure 3.6

A similar procedure was done with the coupled elliptic bursters. Same initial conditions, same level of noise but different noise. In this chase we coupled mutually (all-to-all) 10 bursters. A typical PSTH is in Figure 3.9. Figure 3.10 shows that the firing pattern is reliable.

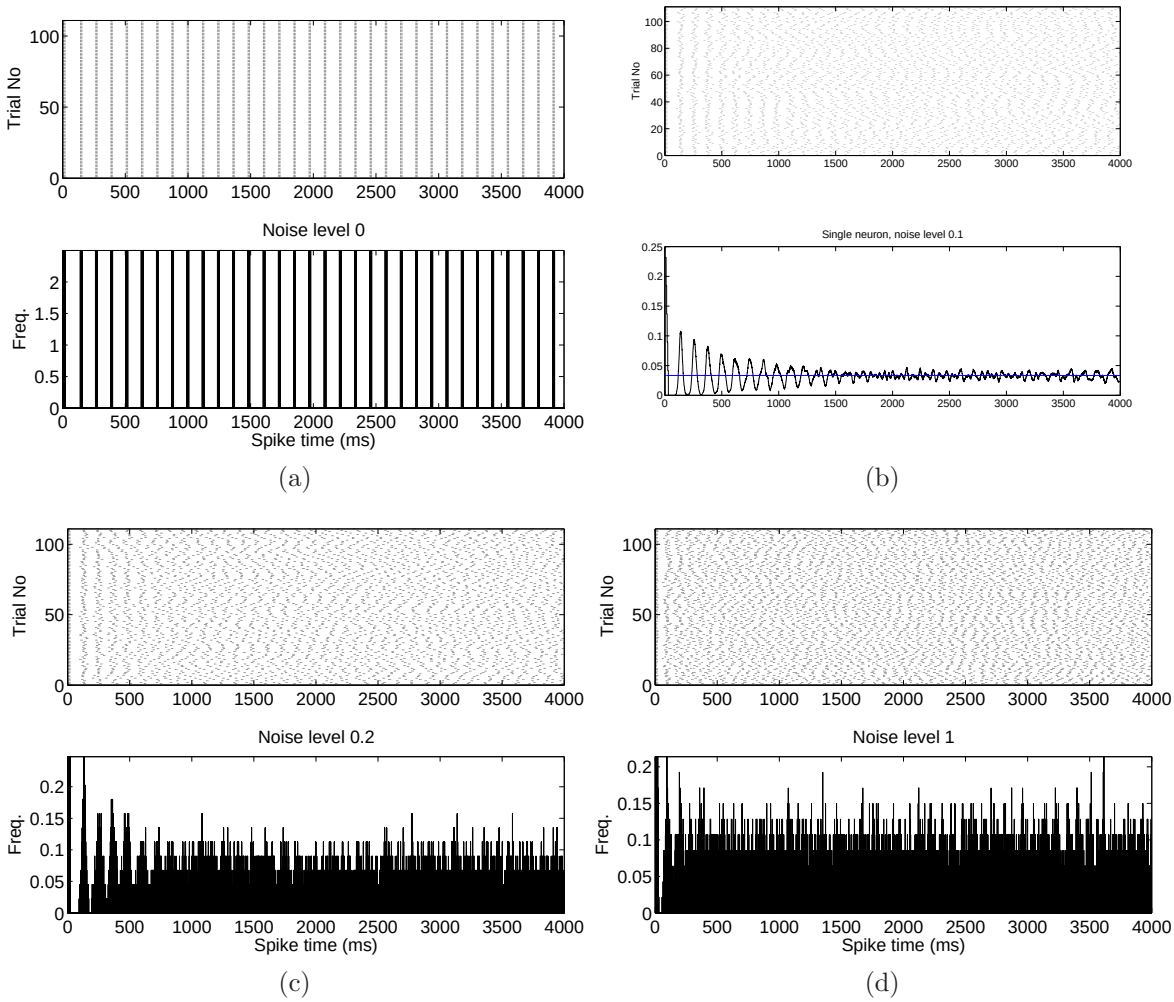

Figure 3.7: Raster plot and PSTH for 100 simulated noisy non coupled elliptic bursters. The upper part is the raster plot of the spike timing and the lower part is PSTH collected over 100 simulated trials. The bin width is 0.64. As a base for the threshold we use the mean

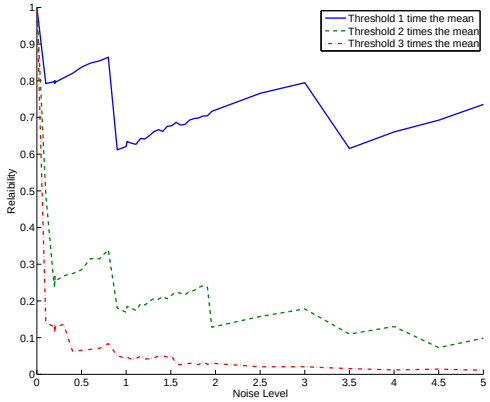

Figure 3.8: Reliability versus noise level for single elliptic bursters

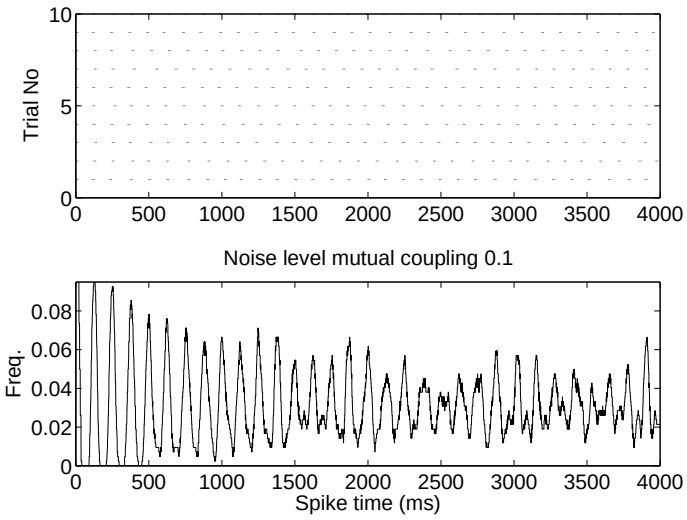

Figure 3.9: PSTH for coupled elliptic bursters

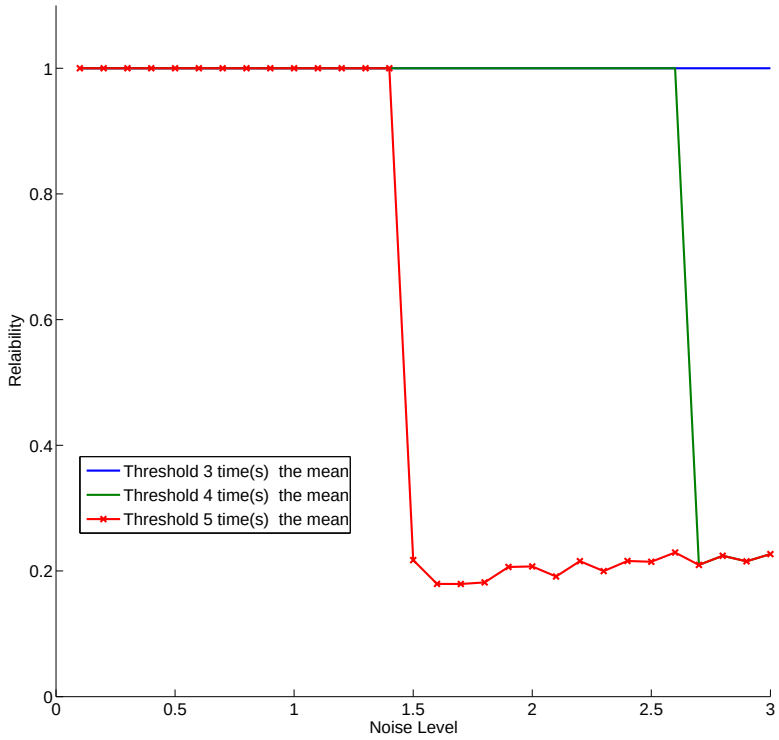

Figure 3.10: Reliability versus noise level for coupled elliptic bursters

CHAPTER 4

A MATHEMATICAL MODEL FOR FOREIGN BODY REACTIONS

4.1 Background

The process of foreign body inflammatory reactions to implants involves complex interactions of many types of cells and proteins and occurs as a sequential cascade of parallel and overlapping chemical processes [13]. During a short but complex initiation period of surface mediated reactions, various tissue growth factors are released. In response to the gradient field of tissue growth factors released in the implant domain, fibroblasts migrate towards the implant from the surrounding tissues and/or proliferate within the fibrinogen absorbed on implant surface. The fibroblasts consequently synthesize chains of amino acids called procollagens, a process that is activated by growth factors, including in particular type- β transforming growth factor (TGFβ) (McDonald 1988 [55], Appling et al. 1989 [3]). The procollagens then get converted into their respective collagens by enzymes (Goldberg [31]). Inactive (latent forms of) TGFβ isoforms are also secreted by many cells (Martin et al. 1992 [54]; Streuli et al. 1993 [84]) and they have a considerably longer half-life than their active forms (Roberts and Sporn 1990 [71]). The implant site contains enzymes which activate latent growth factors and also initiate the stabilization of collagen precursors (Miller and Gay 1992 [56]). Similar to other collagen formation such as dermal wound healing, collagenase is synthesized and secreted by fibroblasts as a zymogen (Stricklin et al. 1978 [85]), but collagen degradation cannot occur until the zymogen is activated. These basic reactions were considered in previous modeling study (Dale et al. 1996 [11]) and their corresponding key features of kinetics were incorporated in our mod-

eling. We refer the interested readers to Dallon et al. (2001) [12] for a survey of the field as well as more bibliographical references.

To further investigate the proliferation and inflammation, we study the relationship of inflammatory reactions with aggregation and active participation of blood cells, which release cell-derived growth factor in the fibrin clot. Of particular interest is the role of macrophage. During phagocytosis, neutrophils arrive first but then quickly subside, they make way for macrophages adhesion. Macrophages tend to remain at a wound or an implant site for a few days to weeks and play multiple roles in inflammation and wound healing [33]. Macrophages clean foreign and debris material; they send chemotactic signals to other cell types that will participate in wound healing and finally they play roles in remodeling of Extracellular matrix (EMC) [58]. They are classified into 3 phenotypes according to their roles in the process. Classically activated macrophages designate the effector macrophages that are produced during cell-mediated immune responses. Two signals, interferon-γ (IFNγ) and tumour-necrosis factor (TNF), resulted in a macrophage population that have enhanced microbicidal or tumoricidal capacity and secret high levels of pro-inflammatory cytokines and mediators. On the other hand, the clearance of apoptotic PMNs by macrophages during inflammation can lead to an inhibition of inflammation, owed in part to the production of transforming growth factor-β (TGFβ) [26]. Wound-healing macrophages can develop in response to innate or adaptive signals through interleukin-4 (IL-4). IL-4 stimulates arginase activity in macrophages, allowing them to convert arginine to ornithine, a precursor of polyamines and collagen, thereby contributing to the production of the extracellular matrix [51]. Regulatory macrophages can also arise during the later stages of adaptive immune responses, the primary role of which dampen the immune response and limit inflammation through production of interleukin-10(IL-10) [32]. Although all three types are observed experimentally in

general wound healing processes, the phagocytes biomaterial interactions are known to be similar (Tang 1997 [96]). These basically relations are also incorporated in our modeling consideration.

Using the quantitative predictive tool, we are able to investigate the all possible pathways of foreign body reaction networks and consider impacts of various tissue growth factors and enzymes. Further, because of a significant precursor of collagens is the formation of fibrin layers that provides the domain for growth factors activations in implant process, an important component of our modeling paper is to test numerically various hypotheses on reactions on plasma or chemically coated bio-materials surface (Tang et al 1998 [97]). Our numerical result indicated trends for these variations, serving as a plausible clue for developing new experiment hypotheses.

We describe our mathematical model that matches with experimental data in Section 4.2, and numerical methods in Section 4.3. In Section 4.4, we illustrate the transient dynamics of foreign body reaction dynamics in pure temporal behavior. The summations and conclusions are in Section 4.5

4.2 Mathematical Modeling

Our model is based on collagen kinetics framework developed by Dale et al 1996 [11] for temporal dynamics that were proposed as models for normal adult and fetal wound healing although here we only consider the pure temporal model. Then we include the new kinetics of foreign body reaction of macrophages. The new dynamics is in a different parametric range and they present different characters. The difference are primarily due to the fact the foreign body reaction due to implantation are deep sub-dermal phenomena, but the wound healing processes are primarily based on dermal wound experimental data. The macrophage further introduced new kinetics to the system.

Table 4.1: Variables in the foreign body reactions (after scaling so they are dimensionless).

$f(x,y,t)$	Fibroblast density
$\beta_1(x,y,t)$	Total TGFβ isoform 1, isoform 2 density
$\beta_3(x,y,t)$	TGFβ isoform 3 density
$l_1(x,y,t)$	Total Latent TGFβ isoform 1, isoform 2 density
$l_3(x,y,t)$	Latent TGFβ isoform 3 density
$e_1(x,y,t)$,$e_2(x,y,t)$,$e_3(x,y,t)$	Generic enzymes type 1, 2, 3 densities
$p_1(x,y,t)$, $p_3(x,y,t)$	Procollagens (latent form of collagens) I and III densities
$c_1(x,y,t)$, $c_3(x,y,t)$	Collagens I and III densities
$z_1(x,y,t)$, $z_3(x,y,t)$	Zymogens (latent forms of collagenases) I and III densities
$s_1(x,y,t)$, $s_3(x,y,t)$	Collagenases I and III densities
$l(x,y,t)$	Macrophage cell density

4.2.1 Chemical Kinetics Equations

We briefly state the modeling consideration for the variable involved, listed in Table 4.1.

Fibroblast density $f(x,y,t)$, represent the main cell type in the implant domain. We ignore the directional effects of the cell and assume the migration are mainly through diffusion. Under tissue growth factor TGFβ (total isoform 1 and isoform 2 density $\beta_1(x,y,t)$, isoform 3 density $\beta_3(x,y,t)$) , the cell population can be approximated by a chemically enhanced logistic growth term, along with a natural decay.

$$\frac{\partial f}{\partial t} = D_1\nabla^2 f + (A_1 + A_2\beta_1 + A_3\beta_3)f\left(1 - \frac{f}{k}\right) - A_4 f \tag{4.1}$$

The fibroblasts are stimulated via autocrine regulation (Roberts & Sporn 1990[71]) to secrete the corresponding latent TGFβ $l_1(x,y,t)$and $l_3(x,y,t)$ with a limiting pro-

duction rate when $l_1(x, y, t)$and $l_3(x, y, t)$ saturates (Wakefield [103]). Latent TGFβ also undergoes an autocrine mechanism, whereby TGFβ induces self-secretion. The concentration of latent growth factor is also decreased because of activation into respective active forms of TGFβ by specific enzymes [7]. Fibroblast proliferation and collagen synthesis are up-regulated by TGFβ s, but by active rather than latent forms (Krummel et al. 1988 [41]). All forms of TGFβ s have constant diffusion coefficients. They are modeled by equations:

$$\frac{\partial l_1}{\partial t} = D_2\nabla^2 l_1 + \frac{A_5 f l_1}{1 + A_6 l_3 + A_7 l_1} - A_8 l_1 - A_{16} e_1 l_1 \tag{4.2}$$

$$\frac{\partial l_3}{\partial t} = D_3\nabla^2 l_3 + \frac{A_9 f l_3}{1 + A_{10} l_3} - A_{11} l_3 - A_{17} e_1 l_3 \tag{4.3}$$

$$\frac{\partial \beta_1}{\partial t} = D_4\nabla^2 \beta_1 + A_{12} e_1 l_1 - A_{13}\beta_1 \tag{4.4}$$

$$\frac{\partial \beta_3}{\partial t} = D_5\nabla^2 \beta_3 + A_{14} e_1 l_3 - A_{15}\beta_3 \tag{4.5}$$

During the early stage of foreign body implantation, monocytes and macrophages release a range of enzymes which activate growth factors, procollagens and zymogens (Sinclair & Ryan 1994[81]). We use the law of mass action to model the activation of latent TGFβ 1 and 3, and type I and type III collagen and collagenases by e_1,e_2,e_3 respectively :

$$\frac{de_1}{dt} = -e_1(A_{16} l_1 + A_{17} l_3) \tag{4.6}$$

$$\frac{de_2}{dt} = -e_2(A_{18}p_1 + A_{19}p_3) + B_{36}l \tag{4.7}$$

$$\frac{de_3}{dt} = -e_3(A_{40}z_1 + A_{41}z_3) \tag{4.8}$$

Procollagen is synthesized by fibroblasts, in response to injury (McDonald 1988 [55]). Further experiments showed up-regulation of procollagen synthesis by active TGFβ (Appling et al. 1989 [3]) hence the inclusion of a linear function of the active TGFβ 1 and 3. We use the law of mass action to model the activation of latent collagens 1 and 3 as well as degradation because of collagenases. The activations of collagenases follow similar mass-action laws under specific enzyme e_3.

$$\frac{dp_1}{dt} = (A_{20} + A_{21}\beta_1 + A_{22}\beta_3)f - A_{23}p_1 - A_{18}e_2p_1 \tag{4.9}$$

$$\frac{dp_3}{dt} = (A_{24} + A_{25}\beta_1 + A_{26}\beta_3)f - A_{27}p_3 - A_{19}e_2p_3 \tag{4.10}$$

$$\frac{dc_1}{dt} = A_{28}p_1e_2 - A_{29}s_1c_1 \tag{4.11}$$

$$\frac{dc_3}{dt} = A_{30}p_3e_2 - A_{31}s_3c_3 \tag{4.12}$$

$$\frac{dz_1}{dt} = \frac{A_{32}}{1 + A_{33}\beta_1 + A_{34}\beta_3}fc_1 - A_{35}z_1 - A_{40}e_3z_1 \tag{4.13}$$

$$\frac{dz_3}{dt} = \frac{A_{36}}{1 + A_{37}\beta_1 + A_{38}\beta_3}fc_3 - A_{39}z_3 - A_{41}e_3z_3 \tag{4.14}$$

$$\frac{ds_1}{dt} = A_{42} z_1 e_3 - A_{43} s_1 + B_{37} l \tag{4.15}$$

$$\frac{ds_3}{dt} = A_{44} z_3 e_3 - A_{45} s_3 + B_{38} l \tag{4.16}$$

Macrophage has been playing multiple roles in foreign body reactions. Our model differs from early collagen model, primarily because we incorporated features (a) macrophages produce procollagens specific enzymes at a near saturated level and (b) macrophage regulate collagen growth through production of zymogens. These changes made substantial new quantitative behavior changes with the model.

The activation and proliferation of macrophage are through upregulation of growth factors TGFβ s [66], but the production does reach a limiting value once TGFβ s reach near saturation. The macrophage cell programmed death normally occurs after several weeks to a month. Here we assume 30 day for convenience.

$$\frac{\partial l}{\partial t} = D_6 \nabla^2 l + B_{39} \left(e_1 l_1 + e_1 l_3 \right) l \frac{(N + Ne)}{N + l} - B_{40} l - B_{41} \sigma_0 \left(t - 30 \right) l \tag{4.17}$$

4.2.2 Model Reduction and Modification

We first consider to reduce the system with the following conditions:

1. The system has no spatial inhomogeneity and therefore no diffusion. So, it becomes a pure temporal model with $D_1 = D_2 = D_3 = D_4 = D_5 = D_6 = 0$.

2. The activation of latent TGFβ 1 and 3, and type I and type III collagen and collagenases reaches equilibrium within a relatively short period of time. We assume that the equations (4.4), (4.5), (4.9), (4.10), (4.13) and (4.14) are in equilibrium.

The system is reduced to 11 equations of Ordinary Differential Equations (ODEs), see Appendix A for details of derivations.

$$\frac{df}{dt} = (A_1 + B_2 e_1 l_1 + B_3 e_1 l_3)\, f \left(1 - \frac{f}{k_1}\right) - A_4 f \tag{4.18}$$

$$\frac{dl_1}{dt} = \frac{A_5 f l_1}{1 + A_6 l_3 + A_7 l_1} - A_8 l_1 - A_{16} e_1 l_1 \tag{4.19}$$

$$\frac{dl_3}{dt} = \frac{A_9 f l_3}{1 + A_{10} l_3} - A_{11} l_3 - A_{17} e_1 l_3 \tag{4.20}$$

$$\frac{de_1}{dt} = -e_1 \left(A_{16} l_1 + A_{17} l_3\right) \tag{4.21}$$

$$\frac{de_2}{dt} = -e_2 f \left(\frac{B_{14} + B_{16} e_1 l_1 + B_{17} e_1 l_3}{A_{23} + A_{18} e_2} + \frac{B_{15} + B_{19} e_1 l_1 + B_{20} e_1 l_3}{A_{27} + A_{19} e_2}\right) + B_{36} l \tag{4.22}$$

$$\begin{aligned} \frac{de_3}{dt} = -\frac{e_3}{\lambda} \Bigg(& \frac{B_{34} f c_1}{(1 + B_{27} e_1 l_1 + B_{28} e_1 l_3)\,(A_{35} + A_{40} e_3)} \\ & + \frac{B_{35} f c_3}{(1 + B_{31} e_1 l_1 + B_{32} e_1 l_3)\,(A_{39} + A_{41} e_3)} \Bigg) \end{aligned} \tag{4.23}$$

$$\frac{dc_1}{dt} = \lambda \left((B_{22} + A_{28} C_3 e_1 l_1 + A_{28} C_2 e_1 l_3)\, f \left(\frac{1000 e_2}{A_{27} + 1000 e_2}\right) - A_{29} s_1 c_1 \right) \tag{4.24}$$

$$\frac{dc_3}{dt} = \lambda \left((B_{24} + A_{30} C_3 e_1 l_1 + A_{30} C_4 e_1 l_3)\, f \left(\frac{1000 e_2}{A_{27} + 1000 e_2}\right) - A_{31} s_3 c_3 \right) \tag{4.25}$$

$$\frac{ds_1}{dt} = \frac{B_{26} f c_1 e_3}{\lambda \left(1 + B_{27} e_1 l_1 + B_{28} e_1 l_3\right) \left(A_{35} + A_{40} e_3\right)} - A_{43} s_1 + B_{37} l \tag{4.26}$$

$$\frac{ds_3}{dt} = \frac{B_{30} f c_3 e_3}{\lambda \left(1 + B_{31} e_1 l_1 + B_{32} e_1 l_3\right) \left(A_{39} + A_{41} e_3\right)} - A_{45} s_3 + B_{38} l \tag{4.27}$$

$$\frac{dl}{dt} = B_{39} \left(e_1 l_1 + e_1 l_3\right) l \frac{(N + Ne)}{N + l} - B_{40} l - B_{41} \sigma_0 \left(t - 30\right) l \tag{4.28}$$

We then proceed to find out parameters in the equations. There are 3 groups of parameters.

The parameter group number 1 consists of well established parameters from measurements: all of them are taken from existing literature. We refer to [10, 23] for details and their related original references. These parameters are not expected to change substantially during different settings of experiments. They are

$$A_1 = 0.72222 \quad B_2 = \frac{A_2 A_{12}}{A_{13}} = 0.5 \quad B_3 = \frac{A_3 A_{14}}{A_{15}} = 0.5 \quad A_5 = 100$$
$$A_9 = 100 \quad A_{16} = 0.1 \quad A_{17} = 0.1 \quad A_{18} = 10$$
$$A_{19} = 10 \quad B_{14} = A_{18} A_{20} = 3$$

$$B_{15} = A_{19} A_{24} = 3 \quad B_{16} = \frac{A_{18} A_{21} A_{12}}{A_{13}} = 1.5 \quad B_{17} = \frac{A_{18} A_{22} A_{14}}{A_{15}} = 3.5 \quad A_{23} = 1$$
$$B_{19} = \frac{A_{25} A_{19} A_{12}}{A_{13}} = 1.5 \quad B_{20} = \frac{A_{26} A_{19} A_{14}}{A_{15}} = 2 \quad B_{22} = A_{28} A_{20} = 5.4 \quad A_{29} = 1$$
$$A_{31} = 1 \quad B_{26} = A_{32} A_{42} = 1.5 \quad B_{27} = \frac{A_{33} A_{12}}{A_{13}} = 1 \quad A_{35} = 10$$
$$B_{30} = A_{36} A_{44} = 4.5 \quad B_{31} = \frac{A_{37} A_{12}}{A_{13}} = 3 \quad B_{32} = \frac{A_{38} A_{14}}{A_{15}} = 1 \quad A_{39} = 10$$
$$A_{40} = 10 \quad A_{41} = 10 \quad B_{34} = A_{40} A_{32} = 50$$
$$B_{35} = A_{41} A_{36} = 50$$

$A_{43} = 1$ $A_{45} = 1$ $k1 = 3.5$ $C_1 = \frac{A_{21}A_{12}}{A_{13}} = \frac{1.5}{A_{18}}$

$C_2 = \frac{A_{22}A_{14}}{A_{28}} = \frac{3.5}{A_{18}}$ $C_3 = \frac{A_{30}A_{25}A_{12}}{A_{13}} = \frac{1.5}{A_{19}}$ $C_4 = \frac{A_{26}A_{14}}{A_{15}} = \frac{2}{A_{19}}$ $B_{36} = 0.005$

$B_{39} = 0.5$ $N = 0$ $Ne = 20$ $B_{40} = 0.001,$

$B_{41} = 8$ $B_{37} = 0$ $B_{38} = 0$

The group number 2 of parameters contains implantation experimental specific constants.

For implantation process, one unique character is that the activation rate from latent collagens to collagens can easily saturate, while there is an abundant amount of e_2. In equations (2.24-2.25) for collagens, we use two steps:

(1) Approximate $\frac{1000e_2}{A_{27}+1000e_2}$ by $\frac{1}{1+10e_2}$ so e_2 does not reach collagen reaction saturation level too quickly. We run the replace system to find out the most fitting curves among the group of parameters in group number 3 below to establish our base parameters for the model.

(2) In final simulation, we resume $\frac{1000e_2}{A_{27}+1000e_2}$ with $A_{27} = 1$ for our purpose. The level 1000 is arbitrarily imposed to ensure the factor being 1 as soon as $e_2 > 0.01$. The purpose of these extra steps is to achieve a better approximation for initial 4 or 5 days of approximation.

The other scaling parameter $\lambda = 0.07$ is the scale factor that make the numerical computed values of collagens 1 and 3 to be at same order of magnitude as experimental data. While our computational result reflects the trend and quantitative features very well in a relative scale level. We have not seen a direct transformation between experimental data and our calculated values. There are a number of factors involved. Typically collagens are measured by count in a specific surface area under microscope (surface density), and out model are more or less in volume density, the distribution in horizontal level is not quite uniform. More accurate collagen measures derive from

measures of hydroxyproline (a constituent of collagen type I), but the scaling factors are not explicitly given also.

The group number 3 of parameters or "selected group" is achieved by numerical simulation to match the experimental data. We pick this group of parameters to fit experiments, because they are subject to change during human development. For example, Dale et al [11] has shown the difference of two groups of values for adult and fetal dermal healing processes.

Based on an experimental data set from Liping Tang's lab (details of experimental setup will be given in upcoming work),

Table 4.2: Experimental data of collagen deposit in a PET membrane.

Collagen deposition on PET 20 um membrane (unit, ug/cm2)					
	#1	#2	#3	#4	#5
4 days	1.5	1.12	0.847	0.957	0.957
7 days	19.63	19.12	20.29	25.8	27.43
14 days	149.96	74.73	89.54	128.82	110.76
21 days	106.32	115.52	140.52	132.94	115.89
28 days	148.32	134.92	179.93	111.8	148.34

we found that the parameter values: $A_6 = 7.5, \quad A_7 = 0.1, \quad A_8 = 15$, $A_{10} = 0.45, \quad A_{11} = 15$, $B_{24} = A_{30}A_{24} = 67.5, \quad B_{28} = A_{34}A_{14} = 202.5$, gave the smallest residual error over all sets of parameters tested. We computed the residual error using the euclidean norm over those time stamps given in the experimental data, 4, 7, 21 and 28 days. We note that, for comparison purpose, the effect of macrophage was not included. This set of parameters is not unique in the sense that different set of parameters yields similar estimations for the total collagen level. For example, changes of $A_{28} \pm 10\%$ does not affect the total collagen level but changes of $A_1 \pm 10\%$

has a significant effect on it. A further analysis is necessary to understand the effect of those changes in the dynamic of the model.

We demonstrate in Figure 4.1 below the comparison of the two data sets and a typical behavior of kinetics for that particular set of parameters, these preliminary results were obtained by the authors in [93], the experimental data and the simulated data from new model with the macrophage density incorporated. The effect of macrophage is to increase the collagen production during the first six days but after that the collagen levels are similar to the Dale's model using our set of parameters up to the 30th day. After 30 days the behavior changes, we have an stabilization in the collagen level for the model we present now which differs with the results in [93] as can be seen in Figure 4.1. Both models agree with the experimental data during the 28-days period.

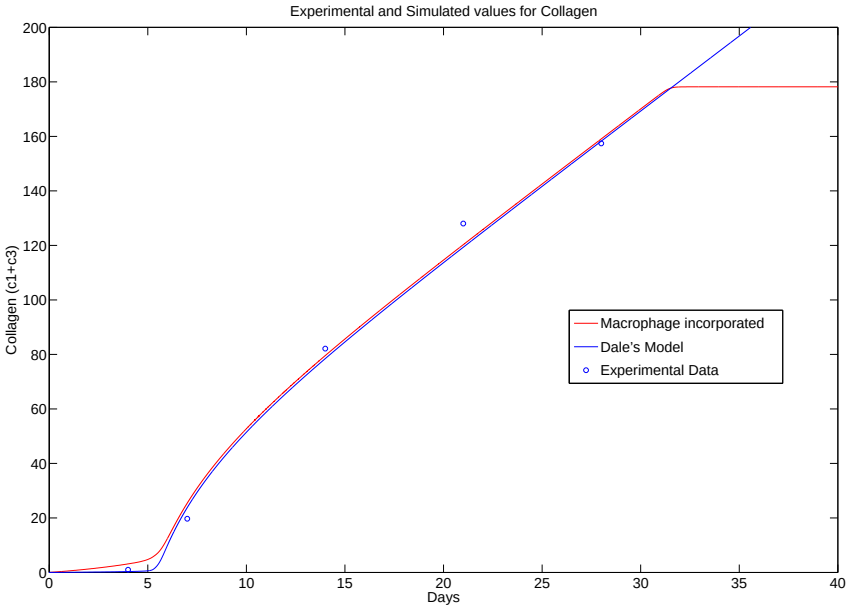

Figure 4.1: The comparison of Collagen of experimental data (the average value of two samples during a 28-day period, unit: up/cm2) with a simulated data from the mathematical model.

4.3 Numerical Methods

We now discuss the numerical solutions for the model we proposed. For the purpose of this research, we did not give rigorous proof for existence or uniqueness of the solution, but simply assume its existence. We also assume that the numerical procedure is stable and numerical solutions converge to exact solution. We did take extra precaution to ensure numerical stability. We, on the other hand, conducted an exhaustive set of standard tests aiming the thorough validation of the numerical scheme and the estimate the truncation error. At last we repeated 4th order Runge-Kutta method using XPPAUT [22] and compared them with our calculation using the full model. The results with the same parameters and the same initial conditions turned out indistinguishable within the order of round-off error.

4.4 Numerical Examples of Collagen Growth

We now show a few numerical experiments of the foreign body reactions that illustrate the general temporal kinetics.

We can see the dynamics of all participating elements in Figure 4.2. We have used the set of parameters estimated above.

1. The effect of initial collagenases changes. The general idea of the experiment is to see if an initial variation of collageneses (by coating implant with collageneses) will alter the collagen deposit level at the end. The numerical simulation gave a negative answer to such a variation (see Figures 4.3 and 4.4).
2. The effect of initial collagen changes. We also found that initial deposit of collagen changes have few impact on the kinetics as well as final collagen layers deposits(see Figure 4.5).

3. The effect of initial enzyme 1 changes. As we continue our numerical experiments to how what are significant factors in the foreign body reaction process, we observed that specific enzyme 1 (which convert latent TGFβ to active TGFβ) plays an important roles. It promotes both TGFβ and fibroblast activations and as well as enzyme 2. In combination of the facts below, that latent TGFβ amounts are not significant factors, we believe there is always abundance of latent TGFβ available but the availability of active TGFβ is a key in a reaction pathway. (see Figure 4.7).
4. Other enzymes are not as significant. We proceed to test the initial level changes at specific enzyme type 2 and specific enzyme type 3 and found the level changes would not cause significant changes in collagen growth(see Figure 4.6).
5. The effect of initial fibroblast changes. As expected, fibroblast is a controlling factor in the foreign body reactions process. Not only the initial fibroblast changes significantly alter levels of collagen deposits, they also change the timing of activations of various elements. Therefore suppression of fibroblast might be crucial in deduction of collagen encapsulations (see Figures 4.8 and 4.4).
6. The effect of latent growth factor TGFβ changes. As discussed earlier, the latent level did not change the kinetics as much, but the conversion to active TGFβs are significant to over all kinetics(see Figure 4.10).

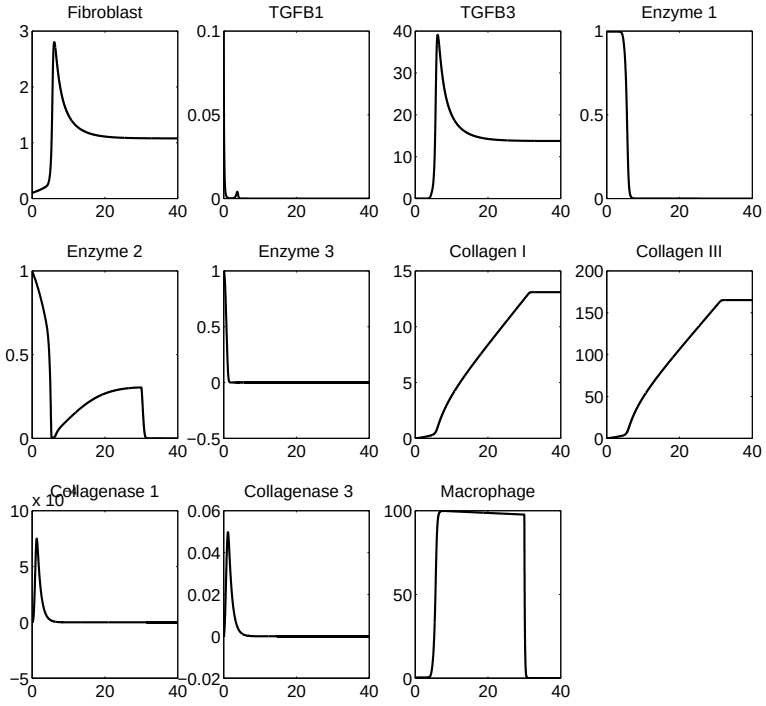

Figure 4.2: The simulated kinetics dynamics of various variables in collagens, procollagens, collageneses, active and latent isoforms of TGFβ etc during first 40 days.

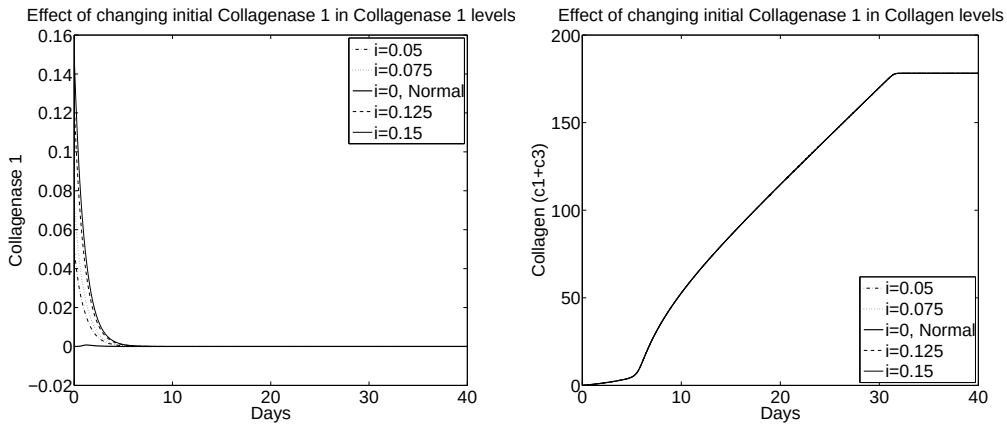

(a) (b)

Figure 4.3: (a) The transient behavior of Collagenese I up to 40 days at different initial levels of Collagenese I, (b) The total collagen level for up to 40 days at different initial levels of Collagenese I

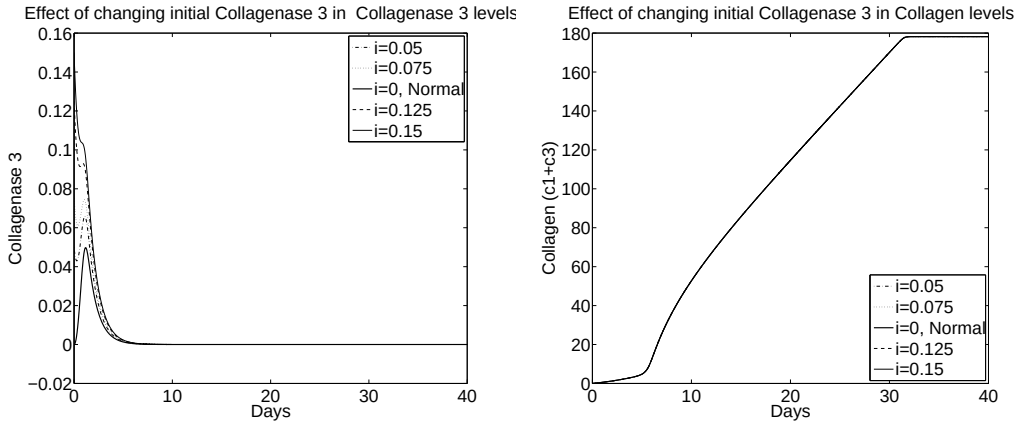

(a) (b)

Figure 4.4: (a) The transient behavior of Collagenese III up to 40 days at different initial levels of Collagenese III, (b) The total collagen level for up to 40 days at different initial levels of Collagenese III.

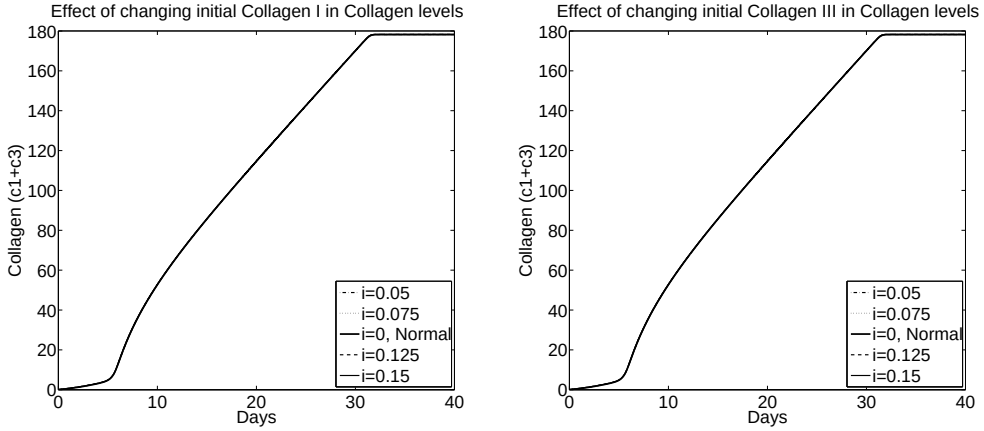

(a) (b)

Figure 4.5: (a) The total collagen level for up to 40 days at different initial levels of Collagen I, (b) The total collagen level for up to 40 days at different initial levels of Collagen III.

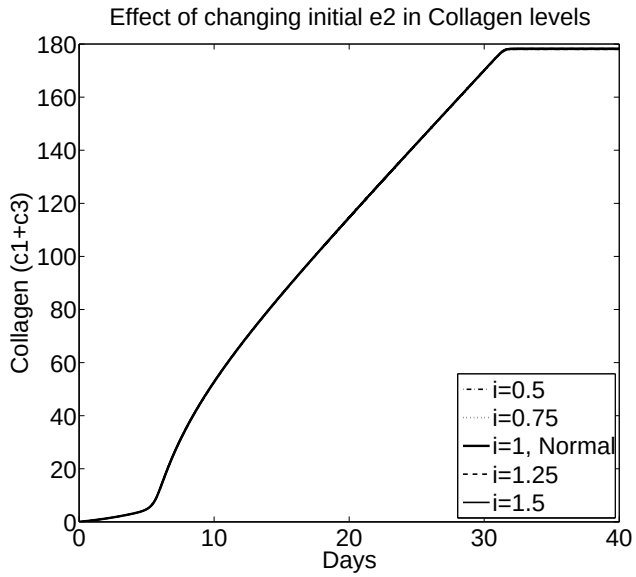

(a)

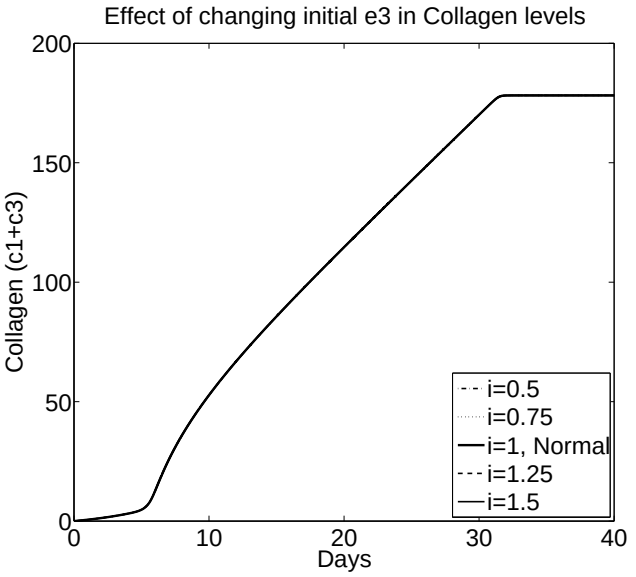

(b)

Figure 4.6: (a) The total collagen level for up to 40 days at different initial levels of enzyme type II, (b) The total collagen level for up to 40 days at different initial levels of enzyme type III.

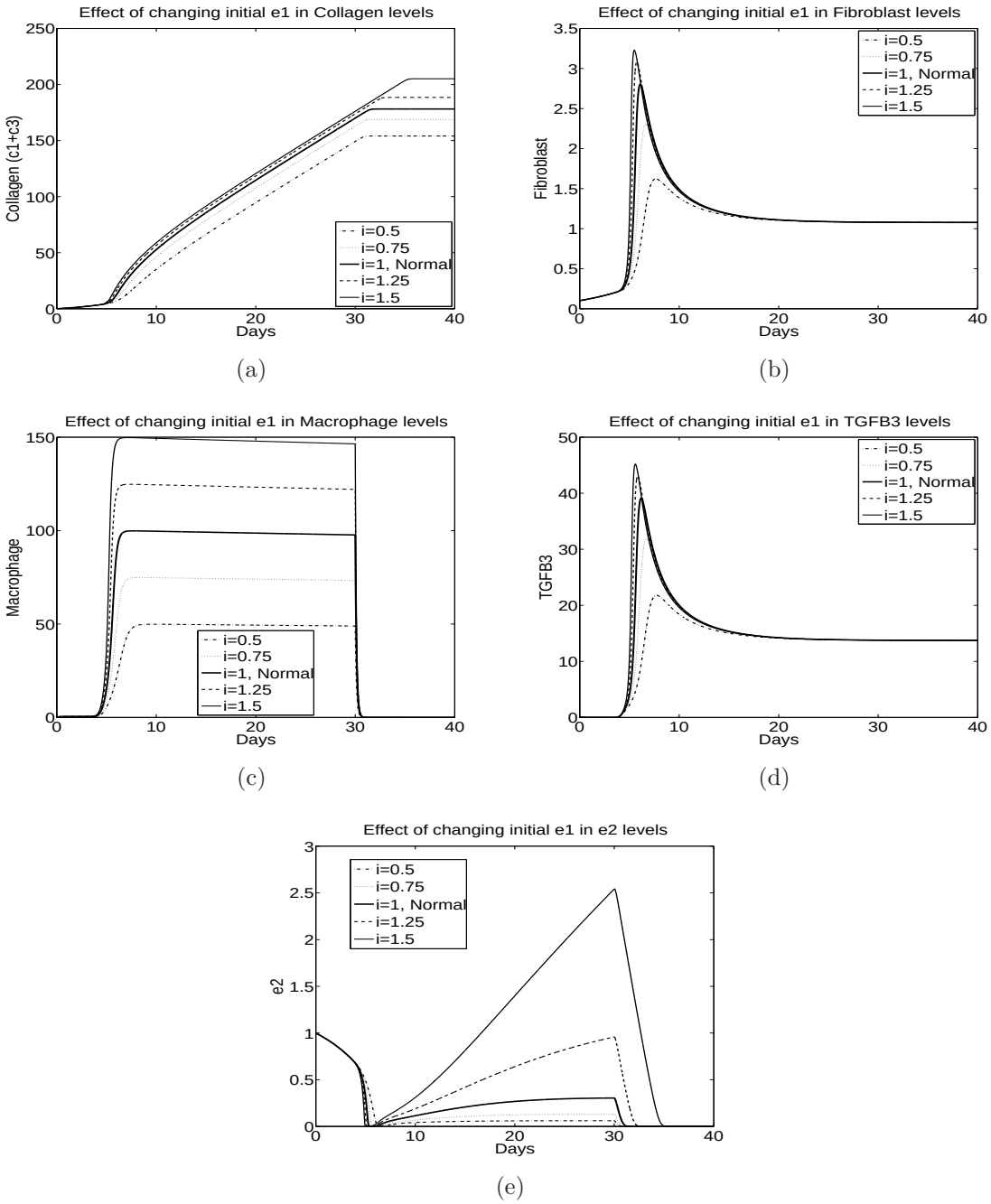

Figure 4.7: (a) The total collagen level for up to 40 days at different initial levels of enzyme type I, (b) The transient behavior of fibroblast up to 40 days at different initial levels of enzyme type I, (c) The macrophage concentration for up to 40 days at different initial levels of enzyme type I, (d) The TGFβ concentration for up to 40 days at different initial levels of enzyme type I, (e) The enzyme type 2 concentration for up to 40 days at different initial levels of enzyme type I.

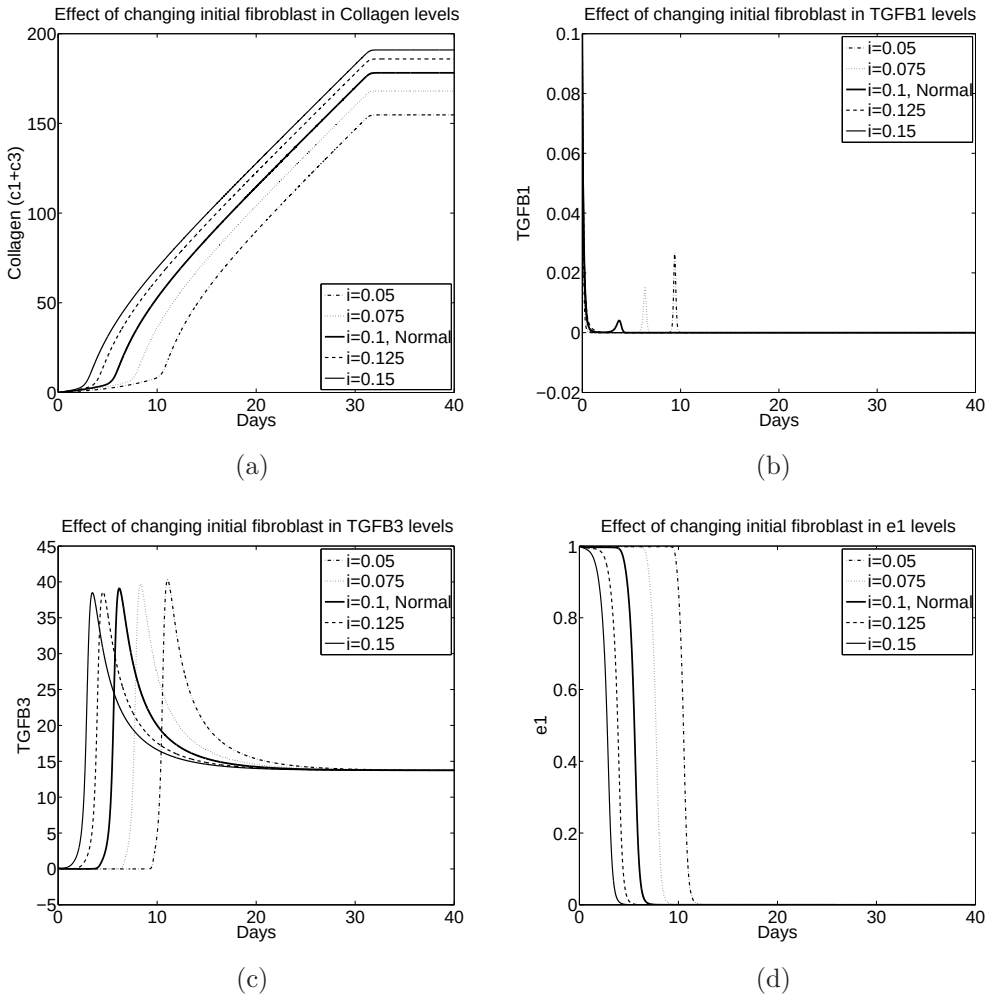

Figure 4.8: (a) The total collagen level for up to 40 days at different initial levels of fibroblast, (b) The transient behavior of TGFβ I concentration up to 40 days at different initial levels of fibroblast, (c) The transient behavior of TGFβ III concentration up to 40 days at different initial levels of fibroblast, (d) The transient behavior of enzyme type I concentration up to 40 days at different initial levels of fibroblast.

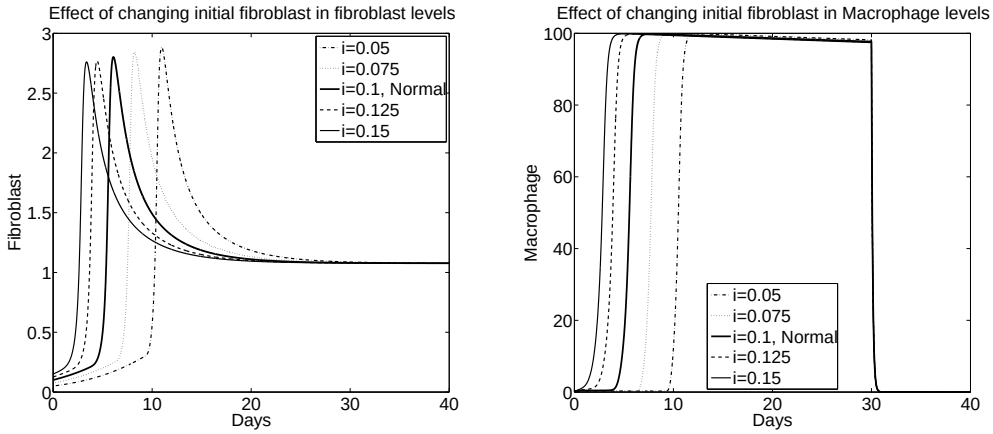

(a) (b)

Figure 4.9: (a) The transient behavior of enzyme type III concentration up to 40 days at different initial levels of fibroblast, (b) The transient behavior of macrophage concentration up to 40 days at different initial levels of fibroblast.

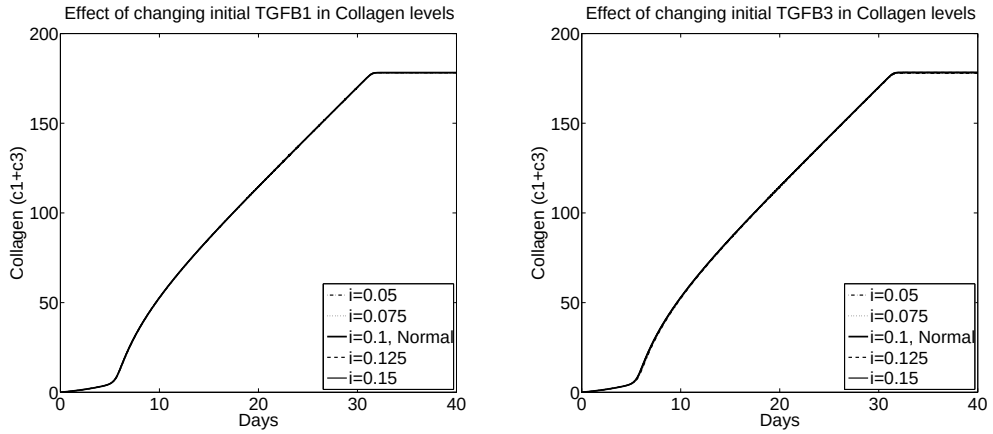

(a) (b)

Figure 4.10: (a) The total collagen level for up to 40 days at different initial levels of latent growth factor TGFβ I, (b) The total collagen level for up to 40 days at different initial levels of latent growth factor TGFβ III.

4.5 Summary and Discussion

The mathematical model has shown its capability to predict some fine features of foreign body reaction process. It has been calibrated to describe temporal and dynamics in the correct order of magnitude. It also confirms that character of collagen growth observed in laboratory experiments.

In a technical level, we found that values of enzyme *e1* and Fibroblast f are very significant to foreign body reactions kinetics, but other variables do not change the kinetics as much. We plan to continue to explore different variation of parameters to observe the full spectrum of changes in kinetics.

APPENDIX A

REDUCTION OF THE SYSTEM (4.18)–(4.28)

We assume that (4.4), (4.5), (4.9), (4.10), (4.13) and (4.14) are in equilibrium. This implies

- $A_{12}e_1l_1 - A_{13}\beta_1 = 0$ or

$$\frac{A_{12}e_1l_1}{A_{13}} = \beta_1$$

- $A_{14}e_1l_3 - A_{15}\beta_3 = 0$ or

$$\frac{A_{14}e_1l_3}{A_{15}} = \beta_3$$

- $(A_{20} + A_{21}\beta_1 + A_{22}\beta_3)f - A_{23}p_1 - A_{18}e_2p_1 = 0$ or

$$\frac{(A_{20} + A_{21}\beta_1 + A_{22}\beta_3)f}{A_{23} + A_{18}e_2} = p_1$$

- $(A_{24} + A_{25}\beta_1 + A_{26}\beta_3)f - A_{27}p_3 - A_{19}e_2p_3 = 0$ or

$$\frac{(A_{24} + A_{25}\beta_1 + A_{26}\beta_3)f}{A_{27} + A_{19}e_2} = p_3$$

- $\frac{A_{32}}{1+A_{33}\beta_1+A_{34}\beta_3}fc_1 - A_{35}z_1 - A_{40}e_3z_1 = 0$ or

$$\frac{\frac{A_{32}}{1+A_{33}\beta_1+A_{34}\beta_3}fc_1}{A_{35} + A_{40}e_3} = z_1$$

- $\frac{A_{36}}{1+A_{37}\beta_1+A_{38}\beta_3}fc_3 - A_{39}z_3 - A_{41}e_3z_3 = 0$ or

$$\frac{\frac{A_{36}}{1+A_{37}\beta_1+A_{38}\beta_3}fc_3}{A_{39} + A_{41}e_3} = z_3$$

After replacing the previos values of $\beta_1, \beta_3, p_1, p_3, z_1$, and z_3 we obtain the reduced system (4.18)–(4.28). Here we used lower case for the coefficients to indicate that do not correpond exactly to those in the system (4.1)–(4.16), rather they repre-

sent dimensionless parameters, normalized by the unwounded levels or aggreations of parameters in the case of B_i or C_i coefficients.

APPENDIX B

CONSTRUCTION OF PSTH HISTOGRAMS

The size of the bin

1. Divide the observation period T into N bins of width Δ, and count the number of spikes k_i from all n sequences that enter the ith bin.
2. Construct the mean and variance of the number of spikes $\{ki\}$.
3. Compute the cost function:

$$C_n(\Delta) = \frac{2kv}{(n\Delta)^2}.$$

4. Repeat 1 through 3 while changing the bin size Δ to search for Δ^* that minimizes $C_n(\Delta)$.

How to build the PSTH

1. Divide the stimulus period or observation period T into N bins of size .
2. Count the number of spikes ki from all n sequences that fall in the bin i.
3. Draw a bar-graph histogram with the bar-height of bin i given by $\frac{k_i}{n\Delta}$ in units of estimated spikes per second at time i Δ.

REFERENCES

[1] H.D.I. Abarbanel, R. Huerta, M.I. Rabinovich, N.F. Rulkov, P.F. Rowat, and AI. Selverston. Synchronized action of synaptically coupled chaotic model neurons. *Neural Computation*, 8(8):1567–1602, 1996.

[2] G. M. Ahlers, C. Cross, P. C. Hohenberg, and S. Safran. The amplitude equation near the convective threshold: application to time-dependant heating experiments. *J. Fluid Mech.*, 110:297–334, 1981.

[3] WD Appling, WR OBrien, DA Johnston, and M Duvie. Synergistic enhancement of type I and III collage production in cultured fibroblast by transforming growth factor - β and ascorbate. *FEBS Letter*, 250(2):541–544, 1989.

[4] V. I. Arnold. Bifurcations and singularities in mathematics and mechanics. In *Theoretical and applied mechanics; Proceedings of the Seventeenth International Congress*, pages 1–25, Amsterdam, 1988. Elsevier Science.

[5] S. M. Baer, T. Erneux, and J. Rinzel. The slow passage through a hopf bifurcation: Delay, memory effects and resonance. *SIAM Appl. Math.*, 49(1):55–71, 1989.

[6] N. Berglund and Gentz B. The effect of additive noise on dynamical hysteresis. *Nonlinearity*, 15:605–632, 2002.

[7] N. Berglund and Gentz B. Pathwise description of dynamic pitchfork bifurcations with additive noise. *Prob. Theory Related Fields*, 122:341–388, 2002.

[8] N. Berglund and Gentz B. Geometric singular perturbation theory for stochastic differential equations. *Journal of Differential Equations*, 191:1–54, 2003.

[9] B. Candelpergher, Diener F., and M. Diener. *Retard à la bifurcation : du local au global*. Springer-Verlag, 1990.

[10] M. C. Cross, P. C Hohenberg, and M. Lucke. Forcing of convection due to time-dependent heating near threshold. *J. Fluid Mech.*, 136:269–276, 1983.

[11] P. D. Dale, J. A. Sherratt, and P. K. Maini. A mathematical model for collagen fibre formation during foetal and adult dermal wound healing. *Proc Biol Sci*, 263(1370):653–660, May 1996.

[12] J. C. Dallon, J. A. Sherratt, and P. K. Maini. Modeling the effects of transforming growth factor-beta on extracellular matrix alignment in dermal wound repair. *Wound Repair Regen*, 9(4):278–286, 2001.

[13] K.C Dee, D.A. Puleo, and R. Bizios. Wound healing. In Hoboken, editor, *An introduction to tissue-biomaterial interactions*, pages 165–214, Hoboken, 2002. John Wiley and Sons.

[14] C-F. Del Negro, C. ans Hsiao, S. Chandler, and A. Garfinkel. Evidence for a novel bursting mechanism in rodent trigeminal neurons. *Biophys. J.*, 75:174–182, 1998.

[15] A. Destexhe, A. Babloyantz, and T. J. Selnowski. Ionic mechanisms for intrinsic slow oscillations in thalamic relay neurons. *Biophy. J.*, 65:1538–1552, 1993.

[16] A. Destexhe, D. A. McCormick, and T. J. Selnowski. A model for 8-10 hz spindling in interconnected thalamic relay and reticularis neurons. *Biophy. J.*, 65:2473–2477, 1993.

[17] M Dhamala, V K. Jirsa, and Ding M. Transitions to synchrony in coupled bursting neurons. *Physical Review Letters*, 93(22):028101, 2004.

[18] F. Diener and M. Diener. Sept formules relatives aux canards. *C. R. Acad. Sci. Paris*, 297:577–580, 1983.

[19] F. Diener and M. Diener. Maximal delay. *Dynamical bifurcation (E. Beniot, editor), Springer, lecture notes in math.*, 1493:71–86, 1993.

[20] Rubin J. E. Bursting induced by excitatory synaptic coupling in non-identical conditional relaxation oscillators or square-wave bursters. Technical Report 06-08, University of Pittsburgh, Technical report 06-08, http://www.math.pitt.edu/techreports.html, 2006.

[21] B. Ermentrout. *Simulating, Analyzing, and Animating Dynamical Systems.* SIAM, Philadelphia, 2002.

[22] B. Ermentrout. *Simulating, Analyzing, and Animating Dynamical Systems.* SIAM, Philadelphia, 2002.

[23] T. Erneux and D. Mandel. Stationary, harmonic and pulsed operations of an optically bistable laser with saturable absorber, II. *Phy. Rev. A*, 30 (no.4):1902–1909, 1984.

[24] T. Erneux and D. Mandel. Imperfect bifurcation with a slowly-varying control parameter. *SIAM. J. Appl. Math.*, 46:1–16, 1986.

[25] T. Erneux and D. Mandel. Slow passage through the laser first threshold: influence of the initial condition. *Optics Comm.*, 85, 1991.

[26] V. A. Fadok, D. L. Bratton, A. Konowal, P. W. Freed, J. Y. Westcott, and P. M. Henson. Macrophages that have ingested apoptotic cells in vitro inhibit proinflammatory cytokine production through autocrine/paracrine mechanisms involving tgf-beta, pge2, and paf. *J Clin Invest*, 101(4):890–898, Feb 1998.

[27] N. Fenichel. Persistence and smoothness of invariant manifolds for flows. *Indiana Univ. Math. J.*, pages 193–226, 1971.

[28] Fruchard. Canards des systems dynamiques discrets. *These de doctorat, U.F.R. de mathematiques de l'Universite Paris 7, F75251 paris Cedex 05*, 1991.

[29] Menon S. V. G. Integral-equation approach to delayed bifurcation in noisy dynamical system. *Phy. Rev. A*, 43 (no.8):4216–4223, 1991.

[30] George Gerstein and Nelson Kiang. An approach to the quantitative analysis of electrophisiological data from single neurons. *Biophysical Journal*, 1, 1960.

[31] B. Goldberg. Kinetics of processing of type i and type iii procollagens in fibroblast cultures. *Proc Natl Acad Sci U S A*, 74(8):3322–3325, Aug 1977.

[32] S. Gordon and P. R. Taylor. Monocyte and macrophage heterogeneity. *Nature Rev. Immunol.*, 5:953–964, 2005.

[33] D. G. Greenhalgh. The role of monocites/macrophages in wound healing. In J. P. Robinson and G. F. Babcock, editors, *Phagocyte function: A guide for research and clinical evaluation*. Wiley-Liss, 1998.

[34] R. Haberman. Slowly-varying jump and transition phenomena associated with algebraic bifurcation problems. *SIAM J. Appl. Math.*, 1979.

[35] Gary R. Holt, WIlliam R. Softky, Christof Kotch, and Rodney Douglas. Comparison of discharge variability in vitro and in vivo in cat visual cortex neurons. *Journal of Neurophysiology*, 75(5), May 1996.

[36] F. Hoppensteadt and E. Izhikevich. *Weakly Connected Neural Networks*. Springer-Verlag, Berlin, 1997.

[37] E. M. Izhikevich. Subcritical elliptic bursting of bautin type. *SIAM Journal on Applied Mathematics*, 60:503–535, 2000.

[38] E. Jakobsson and R. Guttman. Continuous stimulation and threshold of axons: the other legacy of kenneth cole. *"Biophysical approach to excitable system", (ed., W. Adelman and D. Goldman)*, pages 197–211, 1981.

[39] A. K. Kapila. Arrhenius system, dynamics of jump due to slow passage through criticality. *SIAM J. Appl. Math.*, 41:29–42, 1981.

[40] I Karatzas and S. E. Shreve. *Brownian Motion and Stochastic Calculus*. Springer Verlag, New York, 2 edition, 1991.

[41] T. M. Krummel, B. A. Michna, B. L. Thomas, M. B. Sporn, J. M. Nelson, A. M. Salzberg, I. K. Cohen, and R. F. Diegelmann. Transforming growth factor beta (tgf-beta) induces fibrosis in a fetal wound model. *J Pediatr Surg*, 23(7):647–652, Jul 1988.

[42] R. M. Kulkarni and G. S. Ladde. Stochastic perturbations of nonlinear systems of differential equations. *J. Mathematical and Physical Sci.*, 10,no.1:33–45, 1976.

[43] R. Kuske. Probability density for noisy delay bifurcations. *J. Stat. Phys.*, 96:797–816, 1999.

[44] R. Kuske and S. M. Baer. Asymptotic analysis of noise sensitivity in a neuronal burster. *Bulletin of Mathematical Biology*, To appear, 2002.

[45] G. S. Ladde and V. Lakshmikantham. *Random Differential Inequalities*. Academic Press, New York-London, 1980.

[46] N. R. Lebovitz and A. I. Pesci. Dynamic bifurcation in hamiltonian systems with one degree of freedom. *SIAM J. Appl. Math.*, 55 (no.4):1117–1133, 1995.

[47] N. R. Lebovitz and R. J. Schaar. Exchange of stabilities in autonomous systems. *Stud. in Applied Math.*, 54:229–260, 1975.

[48] N. R. Lebovitz and R. J. Schaar. Exchange of stabilities in autonomous systems, II, vertical bifurcation. *Stud. in Applied Math.*, 56:1–50, 1977.

[49] Euiwoo Lee and David Terman. Uniqueness and stability of periodic bursting solutions. *J. Differential Equations*, 158(1):48–78, 1999.

[50] R. Llinas, T. Grace, and Y. Yarom. In vitro neurons in mammalian cortical layer 4 exhibit intrinsic oscillatory activity in the 10- to 50- hz frequency range. *Proc. Nat. Acad. Sci. USA*, 88:897–901, 1991.

[51] P'ng Loke, Iain Gallagher, Meera G Nair, Xingxing Zang, Frank Brombacher, Markus Mohrs, James P Allison, and Judith E Allen. Alternative activation is an innate response to injury that requires cd4+ t cells to be sustained during chronic infection. *J Immunol*, 179(6):3926–3936, Sep 2007.

[52] Zachary F. Mainen and Terrence J. Sejnowsky. Reliability of spike timing in neocortical neurons. *Science, New series*, 268(5216):1503–1506, 1995.

[53] D. Mandel and T. Erneux. Stationary, harmonic and pulsed operations of an optically bistable laser with saturable absorber, I. *Phy. Rev. A*, 30 (no.4):1893–1901, 1984.

[54] P. Martin, J. Hopkinson-Woolley, and J. McCluskey. Growth factors and cutaneous wound repair. *Prog Growth Factor Res*, 4(1):25–44, 1992.

[55] J. A. McDonald. Fibronectin: a primitive matrix. In R. A. F. Clark and P. M. Henson, editors, *The Molecular and Cellular Biology of Wound Repair*, pages 405–436, New York, 1988. Plenum Press.

[56] G.J. Miller and S. Gay. Collagen structure and function. In I.K Cohen, R.F. Diegelmann, and W.J. Lindablad, editors, *Wound Healing: Biochemical and Clinical Aspects*, pages 63–76, Philadelphia, 1992. W.B. Saunders Co.

[57] E.F. Mischenko, Yu. S. Kolesov, A. Yu. Kolesov, and N. Kh. Rozov. *Asymptotic Methods in Singularly Perturbed Systems*. Plenum Press, New York, 1994.

[58] David M Mosser and Justin P Edwards. Exploring the full spectrum of macrophage activation. *Nat Rev Immunol*, 8(12):958–969, Dec 2008.

[59] A. I. Neishtadt. Asymptotical study of stability loss of equilibrium under slow transition of two eigenvalues through imaginary axes. *Uspehi Math Nayk*, 40:5:300–301, 1985.

[60] A. I. Neishtadt. On delayed stability loss under dynamical bifurcations I. *Differential Equations*, 23:1385–1390, 1987.

[61] A. I. Neishtadt. On delayed stability loss under dynamical bifurcations II. *Differential Equations*, 24:171–176, 1988.

[62] A. I. Neishtadt. Averaging and passage through resonances. *Proceedings of the International Congress of Mathematicians, Kyoto, Japan, 1990*, pages 1271–1283, 1991.

[63] A. I. Neishtadt. On calculation of stability loss delay time for dynamical bifurcations. In D. Iagoluitzer, editor, *Proceedings of the International Congress of Mathematical Physics, 1994*, pages 280–287. International press, 1995.

[64] A. I. Neishtadt, C. Simo, and D. V. Treschev. On stability loss delay for a periodic trajectory. *Progress in nonlinear diff. equations and their appl.*, 19:253–278, 1996.

[65] Lionel G. Nowak, Maria V. Sanchez-Vives, and David A. McCormick. Influence of low and high frequency inputs on spike timing in visual cortical neurons. *Cerebral Cortex*, 7:487–501, 1997.

[66] M. R. Owen and J.A. Sherratt. Mathematical modelling of macrophage dynamics in tumours. *Math. Models Meth. Appl. Sci.*, 9(9):513–539, 1999.

[67] L. S. Pontryagin and L. V. Rodygin. Approximate solution of a system of ordinary differential equations involving a small parameter in the derivatives. *Soviet Math. Dokl.*, 1:237–240, 1960.

[68] J. Rinzel. A formal classification of bursting mechanisms in excitable systems. In A. M Gleason, editor, *Proceedings of International Congress of Mathematics*, pages 1578–1593. AMS, 1987.

[69] J. Rinzel and S. M. Baer. Firing threshold of the hodgkin-huxley model for a slow current ramp: a memory effect and its dependence on fluctuations. *Biophys. J.*, 54:551–555, 1988.

[70] J. Rinzel and B. Ermentrout. Analysis of neural excitability and oscillations. *Methods in neuronal modeling: from Ions to networks, 2nd edn. (ed., Koch, C. and Segev, I.)*, pages 251–291, 1998.

[71] A.B. Roberts and M.B Sporn. The transforming growfactors -β's. In M. B. Sporn and A.B. Roberts, editors, *Peptide growth factors and their receptors*, pages 419–472, Berlin, 1990. Springer-Verlag.

[72] J Rubin and Terman D. Geometric singular perturbation analysis of neuronal dynamics. *Handbook of dynamical systems, vol. 2 (ed., Fiedler, B.)*, pages 93–146, 2002.

[73] J. Rubin and D. Terman. Geometric singular perturbation analysis of neuronal dynamics. In B. Fiedler, editor, *Handbook of dynamical systems*, volume 2, pages 93–146. Elsevier Science, 2002.

[74] N.F. Rulkov. Regularization of synchronized chaotic bursts. *Physical Review Letters*, 86(1):183–186, 2001.

[75] J. A. Sanders and F. Verhulst. *Averaging Methods in Non Linear Dynamical Systems*. Springer-Verlag, New York, 1985.

[76] J. A. Sanders and F. Verhulst. *Averaging methods in nonlinear dynamical systems*. Springer-Verlag, New York, 1985.

[77] S. Schecter. Persistent unstable equilibria and closed orbits of a singularly perturbed equation. *Journal of Differential Equations*, 60 (No. 1):131–141, 1985.

[78] A. Sherman and J. Rinzel. Rhythmogenic effects of weak electrotonic coupling in neuronal models. In *Proc. Natl. Acad. Sci.*, volume 89, pages 2471–2474, 1992.

[79] Hideaki Shimazaki and Shigeru Shinomoto. A method for selecting the bin size of a time histogram. *Neural Computation*, 19:1503–1527, 2007.

[80] M. A. Shishkova. Examination of a system of differential equations with a small parameter in the highest derivatives. *Soviet Math. Dokl.*, 14 (No. 2):384–387, 1973.

[81] R. D. Sinclair and T. J. Ryan. Proteolytic enzymes in wound healing: the role of enzymatic debridement. *Australas J Dermatol*, 35(1):35–41, 1994.

[82] D. Somers and N. Kopell. Rapid synchronization through fast threshold modulation. *Biol. Cybern.*, 68:393–407, 1993.

[83] N. G. Stocks, R. Manella, and P.V. E. McClintock. Influence of random fluctuations on delayed bifurcation: the case of additive white noise. *Phys. Rev. A*, 40:5361–5369, 1989.

[84] C. H. Streuli, C. Schmidhauser, M. Kobrin, M. J. Bissell, and R. Derynck. Extracellular matrix regulates expression of the tgf-beta 1 gene. *J Cell Biol*, 120(1):253–260, Jan 1993.

[85] G. P. Stricklin, A. Z. Eisen, E. A. Bauer, and J. J. Jeffrey. Human skin fibroblast collagenase: chemical properties of precursor and active forms. *Biochemistry*, 17(12):2331–2337, Jun 1978.

[86] J. Su. Delayed oscillation phenomena in the fitzhugh nagumo equation. *Journal of Differential Equations*, 105(1):180–215, 1993.

[87] J. Su. On delayed oscillations in nonspatially uniform fitzhugh nagumo equation. *Journal of Differential Equations*, 110 (1):38–52, 1994.

[88] J. Su. Delayed bifurcation properties in the fitzhugh nagumo equation with periodic forcing. *Differential and Integral Equations*, 9 (no.3):527–539, 1996.

[89] J. Su. Persistent unstable periodic motions, I. *Jour. of Math. Anal. Appl.,*, 198:796–825, 1996.

[90] J. Su. Persistent unstable periodic motions, II. *Jour. of Math. Anal. Appl.*, 199:88–119, 1996.

[91] J. Su. Effects of periodic forcing on delayed bifurcations. *Jour. of Dynamics and Differential Equations*, 9 (4):561–625, 1997.

[92] J. Su, J. Rubin, and D. Terman. Effects of noise on elliptic bursters. *Nonlinearity*, 17:133–157, 2004.

[93] Jianzhong Su and Humberto Perez. Modeling and simulation of foreign body reactions to neural implants. In *Advances in Cognitive Neurodynamics: Proceedings of the International Conference on Cognitive Neurodynamics*, pages 879–883. Springer, Nov 2007.

[94] Jianzhong Su, Humberto Perez-Gonzalez, and Ming He. Regular bursting emerging from coupled chaotic neurons. In *Discrete and Continuous Dynamical Systems, Supplement*, pages 946–955, 2007.

[95] J. B. Swift, P. C. Hosenberg, and G. Ahlers. Stochastic landau equation with time-dependent drift. *Phys. Rev. A*, 43:6572–6580, 1991.

[96] Liping Tang, S. Welty, Smith C. W., and J. W. Eaton. Participation on adhesion molecules in inflamatory responses to biomaterials. *Trans. Soc. Bio. Mater.*, 23:261, 1997.

[97] Liping Tang and Y. Wu. Fibrinogen absorption and host tissue responses to plasma functionalized surfaces. *J. Biomed. Marter. Res.*, 1:156–163, 1998.

[98] D. Terman. Chaotic spikes arising from a model of bursting in excitable membranes. *J. Appl. Math.*, 51(5):1418–1450, 1991.

[99] D. Terman. Chaotic spikes arising from a model of bursting in excitable membranes. *SIAM J. Appl. Math.*, 51 (5):1418–1450, 1991.

[100] D. Terman. The transition from bursting to continuous spiking in excitable membrane models. *J. Nonlinear Sci.*, 2 (2):135–182, 1992.

[101] D. Terman, N. Kopell, and Bose A. Dynamics of two mutually coupled slow inhibitory neurons. *Physica D*, 117:241–275, 1998.

[102] D. Terman and D. Wang. Global competition and local cooperation in a network of neural oscillators. *Physica D*, 81:148–176, 1995.

[103] L. M. Wakefield, D. M. Smith, K. C. Flanders, and M. B. Sporn. Latent transforming growth factor-beta from human platelets. a high molecular weight complex containing precursor sequences. *J Biol Chem*, 263(16):7646–7654, Jun 1988.

[104] X.-J. Wang. Ionic basis for intrinsic-40 hz neuronal oscillations. *Neuroreport*, 5:221–224, 1993.

[105] X.-J. Wang and J. Rinzel. Oscillatory and bursting properties of neurons. *Handbook of Brain Theory and Neural networks, (ed., M.A. Arbib)*, pages 686–691, 1995.

[106] H. F. Weinberger and S. Rosenblat. *Forgotten parameters and catastrophic behavior in a stochastic buckling problem*, pages 447–497. Academic Press, 1982.

[107] H. Zeghlache, D. Mandel, and C. Van den Broeck. Influence of noise on delayed bifurcations. *Phy. Rev. A*, 40:286–294, 1989.

BIOGRAPHICAL STATEMENT

Humberto D. Perez Gonzalez was born in Corozal, Colombia, in 1971. He received his B.S. in Mathematics degree from Universidad de Sucre, Colombia, in 1996. In 2002 he received a degree of Specialist in Advance Mathematics from Universidad de Cartagena in Colombia. Then he went to Puerto Rico to get a M.S. degree in Pure mathematics from University of Puerto Rico at Mayagüez in 2006. He joined the doctoral program in the Department of Mathematics, University of Texas at Arlington in Fall 2005. From 1997 to 2002 he worked as part time lecturer in the Universidad de Cartagena where he also worked as Young Researcher sponsored by COLCIENCIAS. The current research are focused on computational and analytic study of neuron and fibrosis dynamics. The long term research interest is to use computational simulations and bifurcation analysis to study the biophysical dynamics at cellular level, the effect of noise and its application to biological systems. Also of interest are using computational or statistical tools for discovery signal transduction pathways of cellular dynamics network.